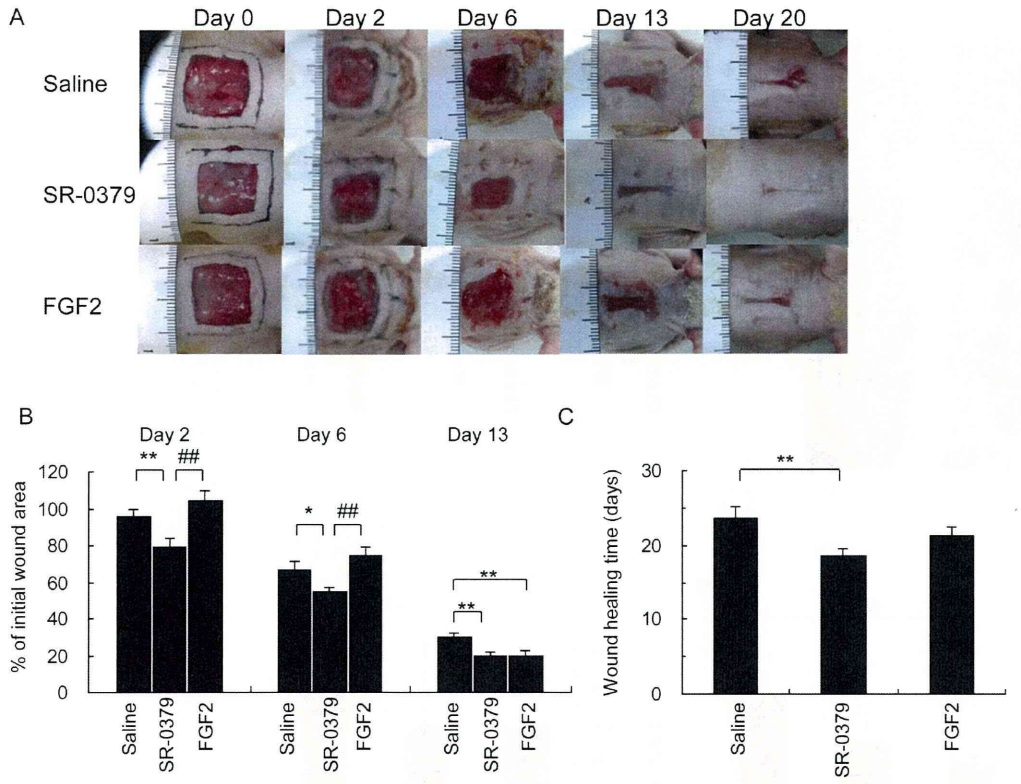

Figure 4. Effects of SR-0379 and FGF2 on full-thickness wound model with flap in diabetic rat model. A) Representative pictures of skin flaps in the streptozotocin-induced diabetic model in the saline (control), SR-0379 (0.2 mg/ml) and FGF2 groups (0.06 mg/ml) on days 0, 6, 13 and 20. B) Quantification of the wound area is represented as a percentage of the initial wound area. N = 6 per group. **P<0.01 vs. control, ##P<0.01 vs. FGF2. C) Days to complete healing by the contraction of full-thickness skin flaps in the streptozotocin-induced diabetic model.
doi:10.1371/journal.pone.0092597.g004

stimulate human umbilical vein endothelial cells (HUVECs) proliferation and tube formation at a level similar to AG30/5C. This smaller peptide led to a reduced cost of peptide synthesis. In the previous reports, the replacement with the D-form amino acid improved the proteolytic resistance of antimicrobial peptides [18]. For example, the D-amino acid variants of host defense peptide chicken cathelicidin-2 showed enhanced stability in human serum, and fully resistant to proteolysis by trypsin and bacterial proteases. The modifications increase the stability and lower cytotoxicity of the peptides without altering their antimicrobial potency. We also confirmed the degradation by the peptide bond cleavages in N-terminus of SR-0379, and the change from L-lysine to D-lysine (SR-0379) increased the resistance to serum. Importantly, SR-0379 displayed broader antibacterial activity than the original AG30 and SR-0007. The bactericidal action of antimicrobial peptides such as pexiganan is thought to result from irreversible membrane-disruptive damage [19] [20] [21]. Especially, from the mechanisms of antibacterial activity, SR-0379 exhibited the same MIC against drug-resistant strains, such as aminoglycoside-, carbapenem- and fluoroquinolone-resistant *P. aeruginosa* and MRSA and the multidrug-resistant *A. baumannii*. SR-0379 might be useful to prevent infection by these drug-resistant bacteria.

In vitro experiments with SR-0379 demonstrated the induction of proliferation, tube formation, migration and contraction. The closure of cutaneous wounds involves three processes: epithelization, connective-tissue deposition and contraction. In particular, contraction is one of the main factors contributing to epidermal wound healing [22]. The fibroblast-collagen matrix contraction model provides a unique way to study mechanisms. Treatment with SR-0379 promoted contraction in this model, which corresponds to wound healing. The stimulatory effect of SR-0379 on the wound healing process was also confirmed by two *in vivo* wound-healing models. Furthermore, SR-0379 was able to induce angiogenesis and granulation tissue formation in the paper disc model and collagen production and proliferation in the incised wound rat model. These results support the potential use of SR-0379 in the wound-healing process. The ulcer model with infection is a unique model that is especially close to a clinical situation. Importantly, SR-0379 treatment resulted in rapid healing without infection compared to FGF2.

Although the multiple functions of antimicrobial peptides are well known, the mechanisms are still unclear. For example, LL-37 is often reported in the analysis of FPR2 (formerly known as FRPL1), the promiscuous Pertussis Toxin (PTX)-sensitive GPCR and the purinergic receptor P2X7 and in the transactivation of epidermal growth factor receptor (EGFR) [3]. The activation of EGFR in epithelial cells, endothelial cells and fibroblasts by LL-37 resulted in activation of the p38 MAPK, ERK1/2 MAPK, NFkB and PI3 kinase pathways. In contrast, although we also examined the contribution of P2X7 receptors to the effect of SR-0379, the specific antagonist of P2X7 (Brilliant Blue G) failed to inhibit the effects of SR-0379 (data not shown). SR-0379 also weakly activated EGFR. Interestingly, SR-0379 strongly activated FAK, while an integrin inhibitor (RGD peptide) blocked the Akt/

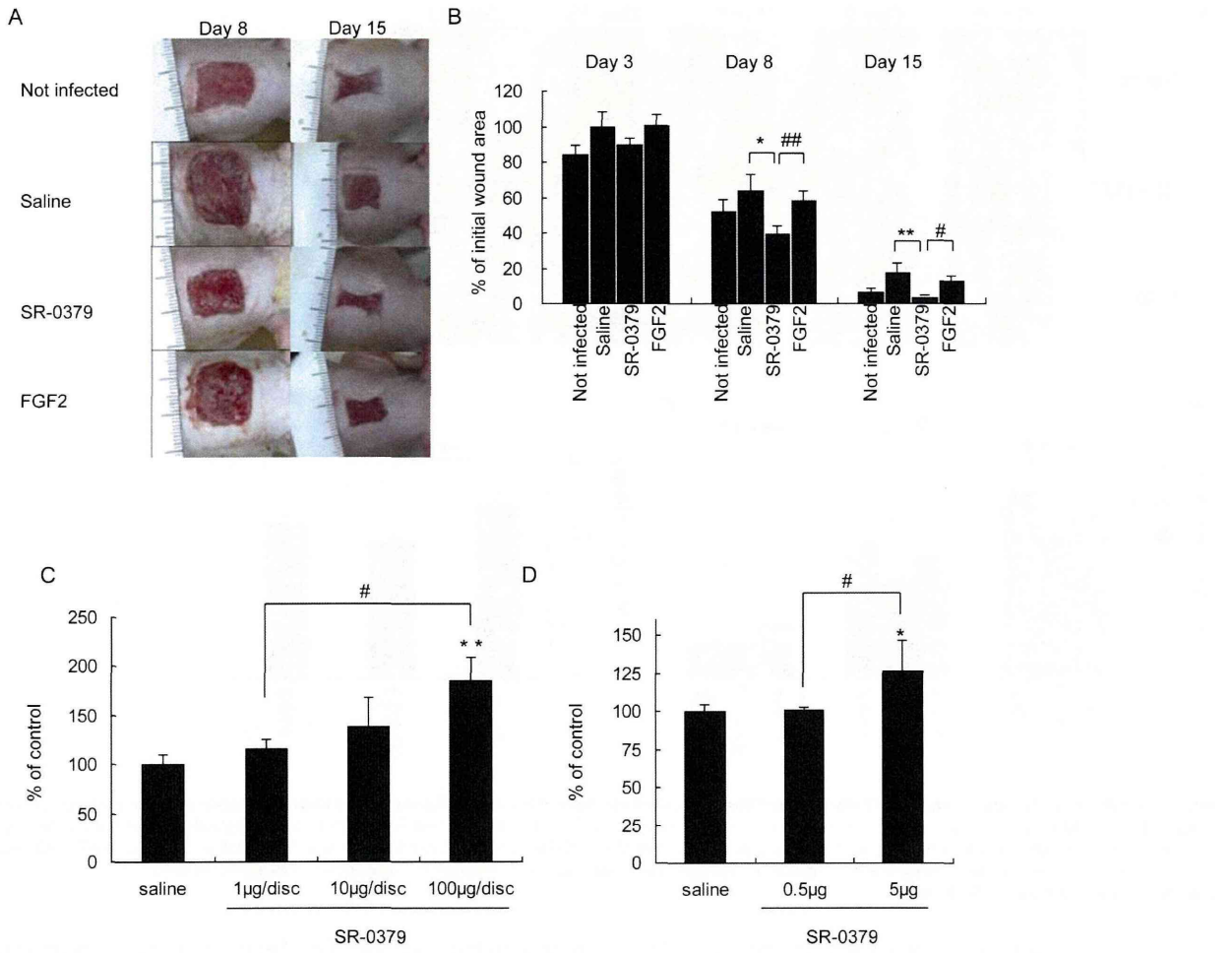

Figure 5. Effects of SR-0379 and FGF2 on the full-thickness skin infected wound model. A) Representative pictures of full-thickness skin flaps in uninfected, saline (control), SR-0379 (1 mg/ml) and FGF2 groups (0.125 mg/ml) on days 8 and 15. B) Quantification of the infected wound area is represented as a percentage of the initial wound area. N = 5 per group. **P<0.01 vs. control, ##P<0.01 vs. FGF2. C) Effects of SR-0379 (1, 10 and 100 μg/disc) on the healing of paper disc implantation in rats. N = 4-5 per group. **P<0.01 vs. control, #P<0.05 vs. 1 μg/disc. D) Effects of SR-0379 (0.5 and 5 μg) on the healing of an experimental open wound in rats. N = 3-4 per group. *P<0.05 vs. control, #P<0.05 vs. 0.5 μg.
doi:10.1371/journal.pone.0092597.g005

mTOR pathway. Downstream of FAK, SR-0379 also activated the PI3 kinase-Akt-mTOR pathway. As mTOR is known to regulate cell growth and survival by integrating nutrient and hormonal signals [10], an inhibitor, rapamycin, attenuated the proliferation induced by SR-0379 in human fibroblasts. The treatment of SR-0379 resulted in increase in cell proliferation of fibroblast, whereas Akt knockdown attenuated the SR-0379-induced cell proliferation These results demonstrate the importance of Akt pathway in the effect of SR-0379.

We have successfully produced SR-0379 as a multifunctional (angiogenic and pro-fibrotic), potent antibacterial peptide with a broad spectrum, including aerobes and anaerobes, Gram-positive and Gram-negative species and drug-resistant and drug-sensitive bacteria and fungi. These properties occur via the activation of PI3 kinase-Akt-mTOR signaling and are useful in the stimulation of wound healing under wet conditions. Further modification of SR-0379 should yield an ideal compound for the treatment of diabetic ulcers, burns and other incurable ulcers. Currently, we plan to test SR-0379 in the treatment of patients with MRSA-positive diabetic and ischemic ulcers.

Materials and Methods

Analysis of the AG30/5C metabolites using MALDI-TOF/MS

Rat sera were collected from rats. AG30/5C was incubated in pooled rat serum at 37°C. Samples were collected before incubation, after 10 minutes of incubation and after 60 minutes of incubation and were precipitated by the addition of an equivalent amount of acetonitrile containing 0.1% trifluoroacetate. The samples were centrifuged, and the supernatants were purified using ZipTip m-C18 (Millipore, MA). Sample solution was mixed with matrix solution (α-cyano 4-hydroxy cinnamic acid). The measurement sample for MALDI (0.4 μL) was applied on a MALDI target plate and dried, and the sequences of the AG30/5C metabolites were confirmed by MALDI-TOF/MS analysis (4700 Proteomics Analyzer, Applied Biosystems, CA).

Serum stability assay

In vitro stability studies were performed by incubating the peptide with rat or human serum. Human sera (Pool of donors, 5 men and 5 women) were commercially purchased from KAC (Kyoto, Japan), which has been permitted only for experiment. We don't use the human biological specimens without the documented informed consent. Rat sera were collected from rats. The peptide (500 μg/ml) was added to serum (300 μL) and incubated at 37°C. A part of samples (90 μL) were taken, and the proteins were precipitated with acetonitrile containing 0.1% trifluoroacetate (200 μL). The precipitate was separated by centrifugation. The supernatants were analyzed by high-performance liquid chromatography (HPLC).

Proliferation, tube formation, cell migration and contraction assays

HUVECs, NHDFs and NHEKs were purchased from Kurabo (Osaka, Japan). The endothelial cells were maintained in HuMedia EB2 and the fibroblasts were maintained in Medium 106S. Both media were supplemented with 1% fetal bovine serum (FBS) as described previously [9]. The epidermal keratinocytes were maintained in HuMedia KB2. Cells were incubated at 37°C in a humidified atmosphere of 95% air/5% CO_2 with exchange of medium every 2 days. HUVECs were cultured in 96-well plates at a density of 10,000 cells/well and incubated for 48 hours at 37°C with AG30/5C or FGF2 (recombinant human FGF basic, R&D systems, Inc., Minneapolis, MN). The proliferation of HUVECs, NHDFs and NHEKs was analyzed using a WST-1 assay (Dojindo, Kumamoto, Japan). Tubule formation assay has recently been developed in which endothelial cells are co-cultured with fibroblasts. An angiogenesis assay kit (Kurabo, Osaka Japan) was used according to the manufacturer's instructions. Various concentrations of peptides or FGF2 were added to the medium. After 11 days, the cells were incubated with diluted primary antibody (mouse anti-human CD31, 1:4,000) for 1 hour at 37°C and diluted secondary antibody (goat anti-mouse IgG alkaline phosphatase-conjugated antibody, 1:500) for 1 hour at 37°C; visualization was achieved with 5-bromo-4-chloro-3-indolyl phosphate/nitro blue tetrazolium (BCIP/NBT). The tube-like structures were measured in terms of total tube length with the software (Angiogenesis Image Analyzer, Kurabo, Osaka Japan). Cell migration was evaluated using an Oris cell migration assay kit (Platypus Technologies, LLC., Madison, WI) according to the manufacturer's instructions. Briefly, the assay utilizes cell-seeding stoppers to restrict cell seeding to the outer annular regions of the wells. Removal of the stoppers reveals a 2-mm diameter unseeded region, the migration zone, into which the seeded cells migrate. The number of cells that migrated into the detection zone was measured using a plate reader. Cellular collagen gel contraction assays were performed as previously described [23] [24]. A solution of collagen and NHDFs (2×10^6 cells/ml) was added to a 24-well plate at 37°C for 1 hour, and medium supplemented with DMEM containing 10% FBS was then added. The cells were cultured for 24 hours. The culture medium was removed, and DMEM (serum-free) containing SR-0379 or FGF2 was added. The cell-embedded matrix was released from the culture dish surface. At each time point, the lattices were digitally photographed from a fixed distance, and their areas were calculated using image analysis software. In the proliferation assay of fibroblast, RGD peptide, Wotmannin, Akt inhibitor IV and Genistein were obtained from Sigma-Aldrich (St. Louis, MO). Rapamycin was obtained from Funakoshi Co., Ltd.(Tokyo, Japan). Akt siRNA I (#6211) and control siRNA I (#6568) were obtain from Cell Signaling (Boston, MA).

NHDFs were plated at a density of 5000 cells per well in 96-well culture plates in the corresponding culture media without antibiotics one day prior to transfection. Lipofectamine RNAi-MAX was purchased from Invitrogen. The lipofectamin (2 μL) was gently added to 100 μL medium and the mixture was incubated for 20 minutes at room temperature. The Akt or Control siRNA was added to the mixture and was incubated for 5 minutes. Transfection complexes were added to each well. NHDFs were incubated for 24 hours at 37°C in a CO_2 incubator and then SR-0379 (10 μg/ml) was added. NHDFs proliferation was analyzed using a WST-1 assay.

Measurement of MICs against Bacteria and Fungi

Antimicrobial activity of the peptides was evaluated against *Escherichia coli* JCM 5491, *Pseudomonas aeruginosa* JCM 6119, *Staphylococcus aureus* JCM2874, *Salmonella* Typhimurium JCM1652, *Acinetobacter baumannii* JCM6841, *Bacteroides fragilis* JCM11019, *Fusobacterium nucleatum* JCM11025, *Penicillium glabrum* JCM22534, *Fusarium solani* JCM11383, *Alternaria alternata* JCM5800 (RIKEN, A research institution for basic and applied science in Japan), *Micrococcus luteus* NBRC13867, *Bacillus subtilis* NBRC3134, *Propionibacterium acnes* NBRC107605, *Trichophyton mentagrophytes* NBRC6124, *Trichophyton rubrum* NBRC9185, *Candida krusei* NBRC1395 (National Institute of Technology and Evaluation, Tokyo, Japan), *Salmonella* Enteritidis IID604 (The Institute of Medical Science, The University of Tokyo, Tokyo, Japan). Additionally, the clinical isolates (Drug-sensitive/resistant *Pseudomonas aeruginosa* and *Staphylococcus aureus*, Osaka University Hospital) and multidrug-resistant *Acinetobacter baumannii* (ATCC BAA-1605) were used. The MICs (expressed as μg/ml) of AG30/5C, SR-0007 and SR-0379 were determined by the broth microdilution method as previously described [8,9]. Serial two-fold dilutions of peptide were added to 0.1 ml of medium containing each type of bacteria and fungi at concentrations of 0.4×10^4 – 5×10^4 CFU/ml. The plates were incubated at 37°C with vigorous shaking for 24 or 48 hours. The MICs were determined as the lowest concentrations of peptide that inhibited visible bacterial growth.

Western blot analysis

Protein extracts (15 μg) were resolved by 10% SDS-PAGE and were then transferred to nitrocellulose membrane. Western blotting was performed. Phospho FAK (Tyr397), Akt, phospho Akt (Ser 473), mTOR, phospho mTOR (Ser2448) and α-Tubulin antibodies were obtained from Cell Signaling (Boston, MA). FAK antibody was obtained from Millipore (Billerica, MA). Phospho FAK (Tyr925) antibody was obtained from Abcam (Cambridge, MA).

Real-time reverse transcription-polymerase chain reaction (RT-PCR) analysis and ELISA

Expression of the human IL-8 mRNA was measured using real-time reverse transcription polymerase chain reaction (RT-PCR). Total RNA was extracted from the tissue samples using ISOGEN reagent (NIPPON GENE, Toyama, Japan). Complementary DNA (cDNA) was synthesized using the Thermo Script RT-PCR System (Invitrogen, Carlsbad, CA). Relative gene-copy numbers for IL-8 mRNA and glyceraldehyde-3-phosphate dehydrogenase (GAPDH) were determined by real-time RT-PCR using TaqMan Gene Expression Assays (IL-8: Hs00174103_m1; GAPDH: 4352934). Absolute gene-copy numbers were normalized to GAPDH using a standard curve.

The cell free culture supernatants were harvested after treatment of SR-0379 (1, 3 and 10 μg/ml) at 24, 48 and 72 hours.

The amount of IL-8 was measured by enzyme-linked immunosorbent assay (ELISA) (R&D Systems, Minneapolis, MN, USA) according to the manufacturer's instructions.

Effect of SR-0379 on wound healing in a streptozotocin-induced diabetic model

This experimental protocol was approved by the committee for ethics in animal studies of AnGes MG. Male HWY/Slc rats (7 weeks) were given a single intravenous injection of 65 mg/kg streptozotocin (STZ, Sigma-Aldrich, St. Louis, MO), and whole-blood glucose was monitored 24 hours later. This strain is hair less in adult and suitable for wound healing model. The glucose level criterion for diabetes was set at 300 mg/dl. STZ-induced diabetic rats were anesthetized. The square flap (1.73 cm × 1.73 cm) was made in the back of rats. In the center of the flap, the square wound (1.41 cm × 1.41 cm) with full-thickness defect was made (area per wound; 2 cm^2). In the flap model, skin was cut in three directions of square wound to partially block the blood flow to wound. SR-0379 (0.2 mg/ml, 50 µl), FGF2 (0.06 mg/ml, 50 µl) or saline (control) was administered to each wound (each time point from day 0 to 28). Dressings (Perme-roll, Nitto Denko, Japan) were applied to the wounds. We took a picture of wound with scale every time and calculated the size of scanned image using software (http://hp.vector.co.jp/authors/VA004392/Download.htm#lenara).

Effect of SR-0379 on wound healing in a cyclophosphamide-induced immunodeficient infection model

Male HWY/Slc rats (7 weeks) were given a single intravenous injection of 100 mg/kg cyclophosphamide (CPA, Wako Pure Chemical Industries, Ltd., Osaka, Japan) and were anesthetized for the preparation of a full-thickness skin flap 24 hours later. CPA-treated rats with white blood cell counts lower than 5,000 were used. The bacteria (*S. aureus*, 1×10^5 CFU/ml) was applied to each wound on days 0, 1, 2 and 3. SR-0379 (1 mg/ml, 50 µl), FGF2 (125 µg/ml, 50 µl) and saline (control, 50 µl) were administered to the wound at time points on days 0 to 27. Dressings (Perme-roll, Nitto Denko, Japan) were applied to the wounds. Healing size was evaluated by photographing the wound area at a close and fixed distance. The remaining unhealed wound size was measured from the image.

Evaluation of granulation tissue formation in a paper disc implantation model

Granulation tissue formation was determined as described previously [25]. A paper disc containing saline or SR-0379 (1, 10 and 100 µg) was implanted into the subcutaneous tissue on the backs of 9-week-old Crl:CD(SD) rats under anesthesia. Four or five rats were used for each experimental condition. The paper disc was removed on day 8 and the granulation tissue around the paper disc was weighed after the removal of absorbed fluids with paper wipe.

Evaluation of collagen production and proliferation in the incised wound rat model

The dermises of Crl:CD(SD) rats (7 weeks) were incised under anesthesia. In the back of rats, we cut the skin (30 mm) and sutured 3 points (Nylon thread, Natsume Seisakusho Co., Ltd., Tokyo, Japan). SR-0379 (0.5 and 5 µg per day) was topically administered in sutured wound one a day for 5 days, and during the period the suture was removed at day 3. At day 6, extracted skin was fixed in one side and pulled in another side. The tension was monitored until the opening of sutured wound. In this evaluation, the increase in tension reflects the strength of sutured wound.

Statistical analysis

All values are expressed as the means + SEM. Analysis of variance and a subsequent Fisher's Least Significant Difference test were used to determine the significance of differences in multiple comparisons.

Supporting Information

File S1 Supporting figures S1–S4. Figure S1, MALDI-TOF MS analysis. A) Major metabolites of AG30/5C determined by MALDI-TOF MS. Parent compound (AG30/5C) was incubated with rat serum *in vitro* for 10 minutes and 60 minutes. The metabolites were identified by the comparison with that from pre-incubation. Figure S2, Effect of SR-0379 on cell proliferation. Normal Human Epidermal Keratinocytes (NHEKs) were treated with SR-0379 (1, 3 and 10 µg/ml). The results were shown as percent increase compared with control (no treatment). N = 3 per group. *P<0.05 vs. control. Figure S3, Effect of Akt pathway on SR-0379-induced cell proliferation. A) Knockdown of Akt expression by siRNA was confirmed with western blot analysis anti-Akt antibody and anti-α-tubulin antibody. The sample was extracted from NHDFs with no treatment (NT), non-target siRNA (C: control) and Akt siRNA. B) Effects of Akt inhibitor on NHDFs proliferation stimulated by SR-0379. The cells were preincubated with Akt inhibitor IV (1 µM) for 1 hour and then were treated with SR-0379 (1, 3 and 10 µg/ml). N = 3 per group. *P<0.05 vs. control, **P<0.01 vs. control, ## P<0.01 vs. SR-0379 (1 µg/ml), †† P<0.01 vs. SR-0379 (3 µg/ml), ‡‡ P<0.01 vs. SR-0379 (10 µg/ml). Figure S4, Up-regulation of interleukin-8 (IL-8) induced by treatment of SR-0379. A) IL-8 mRNA expression was quantified by real time PCR and shown as a relative expression compared with that of GAPDH mRNA. NHDFs were treated with SR-0379 (10 µg/ml) for 24 hours. Effects of Wortmannin (PI3kinase inhibitor, 100 nM) and Genistein (Tyrosine-specific protein kinase inhibitor, 100 nM) on SR-0379-induced IL-8 mRNA expression. N = 3 per group. *P<0.05 vs. control, **P<0.01 vs. control, ## P<0.01 vs. SR-0379 (no inhibitor). B) IL-8 levels in culture supernatants form NHDF was measured by ELISA at 24, 48 and 72 hours after treatment. NHDFs were treated with SR-0379 (1, 3 and 10 µg/ml) for 72 hours. N = 2.
(PDF)

Acknowledgments

We thank Ms. Ryoko Sata and Mr. Shintaro Komaba for their technical assistance.

Author Contributions

Conceived and designed the experiments: HN KT YK RM. Performed the experiments: HT HN AT YS T. Kanamori T. Kaga NT. Analyzed the data: HT AT T. Kanamori. Contributed reagents/materials/analysis tools: HT AT T. Kaga. Wrote the paper: HT HN.

References

1. Ganz T, Selsted ME, Szklarek D, Harwig SS, Daher K, et al. (1985) Defensins. Natural peptide antibiotics of human neutrophils. J Clin Invest 76: 1427–1435.
2. Wang G, Li X, Wang Z (2009) APD2: the updated antimicrobial peptide database and its application in peptide design. Nucleic Acids Res. England. pp. D933–937.
3. Vandamme D, Landuyt B, Luyten W, Schoofs L (2012) A comprehensive summary of LL-37, the factotum human cathelicidin peptide. Cell Immunol 280: 22–35.
4. Gordon YJ, Romanowski EG, McDermott AM (2005) A review of antimicrobial peptides and their therapeutic potential as anti-infective drugs. Curr Eye Res. England. pp. 505–515.
5. Hancock RE, Sahl HG (2006) Antimicrobial and host-defense peptides as new anti-infective therapeutic strategies. Nat Biotechnol. United States. pp. 1551–1557.
6. Fox MA, Thwaite JE, Ulaeto DO, Atkins TP, Atkins HS (2012) Design and characterization of novel hybrid antimicrobial peptides based on cecropin A, LL-37 and magainin II. Peptides. United States: Crown 2012. Published by Elsevier Inc. pp. 197–205.
7. Won A, Khan M, Gustin S, Akpawu A, Seebun D, et al. (2011) Investigating the effects of L- to D-amino acid substitution and deamidation on the activity and membrane interactions of antimicrobial peptide anoplin. Biochim Biophys Acta. Netherlands: 2010 Elsevier B.V. pp. 1592–1600.
8. Nishikawa T, Nakagami H, Maeda A, Morishita R, Miyazaki N, et al. (2009) Development of a novel antimicrobial peptide, AG-30, with angiogenic properties. J Cell Mol Med. England. pp. 535–546.
9. Nakagami H, Nishikawa T, Tamura N, Maeda A, Hibino H, et al. (2012) Modification of a novel angiogenic peptide, AG30, for the development of novel therapeutic agents. J Cell Mol Med 16: 1629–1639.
10. Squarize CH, Castilho RM, Bugge TH, Gutkind JS (2010) Accelerated wound healing by mTOR activation in genetically defined mouse models. PLoS One 5: e10643.
11. Ge Y, MacDonald DL, Holroyd KJ, Thornsberry C, Wexler H, et al. (1999) In vitro antibacterial properties of pexiganan, an analog of magainin. Antimicrob Agents Chemother 43: 782–788.
12. Gottler LM, Ramamoorthy A (2009) Structure, membrane orientation, mechanism, and function of pexiganan–a highly potent antimicrobial peptide designed from magainin. Biochim Biophys Acta. Netherlands. pp. 1680–1686.
13. Dyson M, Young S, Pendle CL, Webster DF, Lang SM (1988) Comparison of the effects of moist and dry conditions on dermal repair. J Invest Dermatol 91: 434–439.
14. Woo KY, Coutts PM, Sibbald RG (2012) A randomized controlled trial to evaluate an antimicrobial dressing with silver alginate powder for the management of chronic wounds exhibiting signs of critical colonization. Adv Skin Wound Care. United States. pp. 503–508.
15. Edwards R, Harding KG (2004) Bacteria and wound healing. Curr Opin Infect Dis. United States. pp. 91–96.
16. Akita S, Akino K, Imaizumi T, Tanaka K, Anraku K, et al. (2006) The quality of pediatric burn scars is improved by early administration of basic fibroblast growth factor. J Burn Care Res. United States. pp. 333–338.
17. Wieman TJ, Smiell JM, Su Y (1998) Efficacy and safety of a topical gel formulation of recombinant human platelet-derived growth factor-BB (becaplermin) in patients with chronic neuropathic diabetic ulcers. A phase III randomized placebo-controlled double-blind study. Diabetes Care 21: 822–827.
18. Molhoek EM, van Dijk A, Veldhuizen EJ, Haagsman HP, Bikker FJ (2011) Improved proteolytic stability of chicken cathelicidin-2 derived peptides by D-amino acid substitutions and cyclization. Peptides 32: 875–880.
19. Boman HG (1995) Peptide antibiotics and their role in innate immunity. Annu Rev Immunol 13: 61–92.
20. Hancock RE (1997) Peptide antibiotics. Lancet 349: 418–422.
21. Jacob L, Zasloff M (1994) Potential therapeutic applications of magainins and other antimicrobial agents of animal origin. Ciba Found Symp 186: 197-216; discussion 216–123.
22. Kao HK, Chen B, Murphy GF, Li Q, Orgill DP, et al. (2011) Peripheral blood fibrocytes: enhancement of wound healing by cell proliferation, re-epithelialization, contraction, and angiogenesis. Ann Surg 254: 1066–1074.
23. Grinnell F (2000) Fibroblast-collagen-matrix contraction: growth-factor signalling and mechanical loading. Trends Cell Biol. England. pp. 362–365.
24. Carlson MA, Longaker MT (2004) The fibroblast-populated collagen matrix as a model of wound healing: a review of the evidence. Wound Repair Regen. United States. pp. 134–147.
25. Okumura M, Okuda T, Okamoto T, Nakamura T, Yajima M (1996) Enhanced angiogenesis and granulation tissue formation by basic fibroblast growth factor in healing-impaired animals. Arzneimittelforschung 46: 1021–1026.

The FASEB Journal • Research Communication

Treatment of cerebral ischemia-reperfusion injury with PEGylated liposomes encapsulating FK506

Takayuki Ishii,* Tomohiro Asai,* Dai Oyama,* Yurika Agato,* Nodoka Yasuda,* Tatsuya Fukuta,* Kosuke Shimizu,* Tetsuo Minamino,† and Naoto Oku*,[1]

*Department of Medical Biochemistry, School of Pharmaceutical Sciences, University of Shizuoka, Shizuoka, Japan; and †Department of Cardiovascular Medicine, Osaka University Graduate School of Medicine, Osaka, Japan

ABSTRACT **FK506 (Tacrolimus) has the potential to decrease cerebral ischemia-reperfusion injury. However, the clinical trial of FK506 as a neuroprotectant failed due to adverse side effects. This present study aimed to conduct the selective delivery of FK506 to damaged regions, while at the same time reducing the dosage of FK506, by using a liposomal drug delivery system. First, the cytoprotective effect of polyethylene glycol-modified liposomes encapsulating FK506 (FK506-liposomes) on neuron-like pheochromocytoma PC12 cells was examined. FK506-liposomes protected these cells from H_2O_2-induced toxicity in a dose-dependent manner. Next, we investigated the usefulness of FK506-liposomes in transient middle cerebral artery occlusion (t-MCAO) rats. FK506-liposomes accumulated in the brain parenchyma by passing through the disrupted blood-brain barrier at an early stage after reperfusion had been initiated. Histological analysis showed that FK506-liposomes strongly suppressed neutrophil invasion and apoptotic cell death, events that lead to a poor stroke outcome. Corresponding to these results, a single injection of FK506-liposomes at a low dosage significantly reduced cerebral cell death and ameliorated motor function deficits in t-MCAO rats. These results suggest that liposomalization of FK506 could reduce the administration dose by enhancing the therapeutic efficacy; hence, FK506-liposomes should be a promising neuroprotectant after cerebral stroke.—Ishii, T., Asai, T., Oyama, D., Agato, Y., Yasuda, N., Fukuta, T., Shimizu, K., Minamino, T., Oku, N. Treatment of cerebral ischemia-reperfusion injury with PEGylated liposomes encapsulating FK506. *FASEB J.* 27, 1362–1370 (2013). www.fasebj.org**

Key Words: neuroprotectant · tacrolimus · apoptosis · inflammation · motor function

AFTER RESTORATION OF BLOOD FLOW in cerebral stroke patients, cerebral ischemia-reperfusion (I/R) injury often occurs, resulting in neurological deficits (1, 2). Hence, the development of neuroprotective therapy for this type of injury has been awaited for a better outcome after a cerebral stroke. Although >1000 candidate compounds have shown potency as a neuroprotectant, and >100 of them have been tested in clinical studies in the past, none of them have passed these trials due to insufficiency of medicinal efficacy and to adverse side effects (3, 4). To overcome the present situation, we previously applied the liposomal drug delivery system (DDS) to the treatment of cerebral I/R injury (5). When 100 nm liposomes were intravenously injected immediately after the start of reperfusion, they selectively accumulated in the I/R region, suggesting that drug delivery using liposomes is applicable for treatment of I/R injuries. Moreover, liposomes modified with the antiapoptotic protein asialoerythropoietin significantly suppressed cerebral cell death and improved motor functional deficits induced by I/R injury in transient middle cerebral artery occlusion (t-MCAO) rats by increasing the accumulation of the protein in the injured region compared with the outcome for the free asialoerythropoietin-treated group. This finding offers the possibility that liposomal DDS could be a useful strategy for the treatment of cerebral I/R injury. However, the efficacy of liposomal DDS for treatment of cerebral I/R injuries has been proven for just a single protein, *i.e.*, asialoerythropoietin. Accordingly, more study is needed to reinforce the utility of this therapeu-

Abbreviations: DDS, drug delivery system; DiI-C_{18}, 1,1′-dioctadecyl-3,3,3′,3′-tetramethylindocarbocyanine; DPPC, dipalmitoylphosphatidylcholine; DSPE, distearoylphosphatidylethanolamine; FK506-liposome, polyethylene glycol-modified liposomes encapsulating FK506; HCO-60, polyoxyethylene (60) hydrogenated castor oil; HS, horse serum; ICA, internal carotid artery; I/R, ischemia-reperfusion; IVIS, *in vivo* imaging system; MCA, middle cerebral artery; MPO, myeloperoxidase; NGF, nerve growth factor; PEG, polyethylene glycol; t-MCAO, transient middle cerebral artery occlusion; TTC, 2,3,5-triphenyltetrazolium chloride; TTW, therapeutic time window; TUNEL, terminal deoxyribonucleotidyl transferase (TDT)-mediated dUTP-digoxigenin nick end labeling

[1] Correspondence: Department of Medical Biochemistry, School of Pharmaceutical Sciences, University of Shizuoka, 52-1 Yada, Suruga-ku, Shizuoka 422-8526, Japan. E-mail: oku@u-shizuoka-ken.ac.jp

doi: 10.1096/fj.12-221325

This article includes supplemental data. Please visit *http://www.fasebj.org* to obtain this information.

0892-6638/13/0027-1362 © FASEB

tic strategy. The therapeutic effect of liposomes encapsulating a neuroprotective chemodrug on I/R injury has not been examined yet. Therefore, in this study designed for achieving this purpose and developing a novel neuroprotectant, we prepared polyethylene glycol (PEG)-modified liposomes encapsulating FK506 (FK506-liposomes).

The immunosuppressant FK506 has been widely used to prevent allograft rejections in clinical organ transplantation, and was also recently reported to be a drug candidate for the treatment of acute stroke in animal studies (6–8). Calcineurin is activated by excessive influx of Ca^{2+} into cerebral cells after a cerebral ischemic event, resulting in the induction of nitric oxide, generation of inflammatory cytokines, and the release of cytochrome *c* (9–12). FK506 inhibits the activation of calcineurin by associating with the FK506-binding protein (FKBP) in neuronal cells and glial cells; hence, it shows a neuroprotective effect on experimental stroke models. However, the frequent administration of FK506 required to achieve a good outcome has the risk of developing side effects such as heart deficits and nephrotoxicity. The liposomalization of FK506 is a promising approach for changing the biodistribution and negating the problem of poor water solubility (13, 14). The liposomal formulation of FK506 is as effective as an equal dose of commercial FK506 in preventing the rejection of transplant grafts, but with considerably less nephrotoxicity (14). The efficient delivery of FK506 to ischemic regions by using liposomes might potentially reduce the administration dosage without changing neuroprotective efficacy. In the present study, we assessed the potential of FK506-liposomes as a neuroprotectant against cerebral I/R injury by investigating their cerebral distribution, pharmacological activity, therapeutic effect, and therapeutic time window in t-MCAO rats.

MATERIALS AND METHODS

Animals

Male Wistar rats (170–210 g) were purchased from Japan SLC, Inc. (Shizuoka, Japan). The animals were cared for according to the Animal Facility Guidelines of the University of Shizuoka. All animal procedures were approved by the Animal and Ethics Review Committee of the University of Shizuoka.

Preparation of FK506-liposomes

The lipid composition of FK506-liposomes was dipalmitoylphosphatidylcholine (DPPC) and distearoylphosphatidylethanolamine (DSPE)-PEG (molecular weight of PEG was 2000) in a 20:1 molar ratio. FK506-liposomes were prepared by the following freeze-drying method: FK506 was dissolved in methanol and added to a flask containing the above lipids dissolved in *tert*-butylalcohol. The molar ratio of FK506 to DPPC was 1:50. The solution was lyophilized, and then the lyophilizate was hydrated with PBS (pH 7.4) at 50°C. The liposome solution was freeze-thawed for 3 cycles with liquid nitrogen. Then the particle size of the liposomes was adjusted by extrusion through 100-nm pore-size polycarbonate filters (Nuclepore, Cambridge, MA, USA). Unencapsulated FK506 was removed by ultracentrifugation at 604,000 *g* for 15 min (Hitachi, Tokyo, Japan), and the concentration of FK506 in the liposomes was determined by HPLC (Hitachi). Final liposomal concentration was 10 mM as DSPC. FK506-liposomes were dissolved in tetrahydrofuran, and 20 μl of the solution was injected into an octadecylsilane (ODS) column (TSK gel ODS-80TM, 4.6×150 mm, Tosoh, Tokyo, Japan). The mobile phase consisted of acetonitrile and water (3:2, v/v). HPLC analysis was performed at 60°C and a flow rate of 1 ml/min with UV detection at 214 nm. For the cerebral distribution study, 1,1′-dioctadecyl-3,3,3′,3′-tetramethylindocarbocyanine (DiI-C_{18}; Molecular Probes Inc., Eugene, OR, USA) was mixed with the initial lipid solution for fluorescence labeling of the liposomes.

Cell culture

Pheochromocytoma cells [PC12 cells; European Collection of Cell Cultures (ECACC), Porton Down, UK] were cultured in high-glucose DME medium (Wako, Osaka, Japan) supplemented with streptomycin (100 μg/ml), penicillin (100 U/ml), heat-inactivated 5% fetal bovine serum (FBS; Japan Bioserum, Tokyo, Japan), and 10% horse serum (HS; MP Biomedicals, Solon, OH, USA) at 37°C in a humidified chamber with 5% CO_2. PC12 cells were plated on poly-D-lysine-coated 24-well plates for the WST (viability) assay. These cells were caused to differentiate into nerve-like cells by adding nerve growth factor (NGF) at 100 ng/ml to DME medium containing 0.5% HS. Five days after incubation with NGF, these cells were used for subsequent experiments.

Cell proliferation assays

FK506-liposomes (0.01, 0.1, or 1.0 μM as FK506 dosage) or free FK506 (1.0 μM) were added to differentiated PC12 cells in 24-well plates. H_2O_2 was added to each well to a final concentration of 75 μM at 30 min after addition of the samples. The number of viable cells was measured by using TetraColor One (Seikagaku, Tokyo, Japan). Briefly, TetraColar One solution was added to each well, and the cells were then incubated at 37°C for 3 h in a humidified atmosphere containing 5% CO_2. Absorbance at 450 nm was measured by using a Tecan Infinite M200 microplate reader (Tecan, Männedorf, Switzerland). FK506 was dissolved in ethanol, and the final concentration of ethanol was 0.1% in medium.

t-MCAO rats

Preparation of t-MCAO rats was performed as described previously (15). Briefly, anesthesia was induced with 3% isoflurane and maintained with 1.5% isoflurane during surgery. During surgery, the body temperature of the rats was maintained at 37°C with a heating pad. After a median incision of the neck skin had been made, the right carotid artery, external carotid artery, and internal carotid artery (ICA) were isolated with careful conservation of the vagal nerve. An ~18 mm 4-0 monofilament nylon suture coated with silicon was introduced into the right ICA and advanced to the origin of the MCA to occlude it. Silk thread was used for ligation to keep the filament at the site of insertion into the MCA. After the surgery, the neck was closed; anesthesia was then discontinued. MCAO was performed for 1 h. Success of the surgery was judged by the appearance of hemiparesis and an increase in body temperature (>37.8°C). Reperfusion was started by withdrawing the filament ~10 mm at 1 h after the start of occlusion under isoflurane anesthesia.

Drug administration

Polyoxyethylene (60) hydrogenated castor oil (HCO-60; 200 mg/ml), including 10% ethanol was used as vehicle for free FK506. FK506 or FK506-liposomes were intravenously injected at a single dose of 30, 100, or 300 μg/kg body weight (0.5 ml/rat) immediately after the start of reperfusion. In the therapeutic time window study, the injection time was shifted as indicated in the legend of **Fig. 6**. It was reported earlier that the vehicle has no effect on the outcome of ischemia (6, 16, 17).

Cerebral distribution of FK506-liposomes

PEGylated liposomes and FK506-liposomes were fluorescently labeled with DiI-C_{18} as described above. They were intravenously injected into the t-MCAO rats at the start of reperfusion. The rats were euthanized at 3 or 24 h after the injection, and their brains were sliced into 2-mm-thick coronal sections with a rat brain slicer (Muromachi Kikai, Tokyo, Japan). All sections were put on glass slides, and the fluorescence of DiI was measured with an *in vivo* imaging system (IVIS; Xenogen Corp., Alameda, CA, USA). Thereafter, these sections were embedded in optical cutting temperature (OCT) compound (Sakura, Finetech., CO Ltd., Tokyo, Japan) and then frozen in a dry ice/ethanol bath. These frozen sections were cut into 10-μm ones with a cryostat (HM505E; Microm, Walldorf, Germany) for subsequent immunostaining experiments. Average photon counts in I/R region were calculated from 4 rats at each time.

Immunostaining for CD31

The sections were incubated with 1% bovine serum albumin in PBS for 10 min at room temperature for blocking, and then with biotinylated anti-mouse CD31 rat monoclonal antibody (BD Pharmingen, Franklin Lakes, NJ, USA) for 18 h at 4°C, and thereafter with streptavidin-Alexa fluor 488 conjugates (Molecular Probes Inc.) for 30 min at room temperature. Finally, the sections were mounted with Perma Fluor Aqueous Mounting Medium (Thermo Shandon, Pittsburgh, PA, USA) and observed for fluorescence in the striatum with an LSM microscope system (Carl Zeiss Co., Ltd., Oberkochen, Germany).

Terminal deoxyribonucleotidyl transferase (TDT)-mediated dUTP-digoxigenin nick end labeling (TUNEL) staining

Brains of t-MCAO rats were dissected at 24 h after the injection of FK506-liposomes (100 μg/kg as FK506 dosage), free FK506 (100 μg/kg), PEGylated liposomes (same lipid concentration as FK506-liposomes), or PBS; embedded in optimal cutting temperature (OCT) compound (Sakura Finetek, Torrance, CA, USA); and then frozen in dry ice/ethanol. Frozen sections (10 μm) were prepared by using a cryostatic microtome (HM 505E, Microm, Walldorf, Germany) and were stained with TUNEL reagents supplied in an ApopTag Plus fluorescein *in situ* apoptosis detection kit (Chemicon International, Inc., Temecula, CA, USA), as described below. For fixation of the sections, they were incubated in 4% paraformaldehyde for 15 min at room temperature, and then in ethanol/acetic acid (2:1) solution for 5 min at −20°C. DNA strand breaks were labeled with the digoxigenin-conjugated terminal deoxynucleotidyl transferase enzyme by incubation for 1 h at 37°C. Then, the sections were incubated in antidigoxigenin-fluorescein solution for 30 min at room temperature. Finally, the sections were mounted with Perma Fluor aqueous mounting medium including DAPI (1.0 μg/ml) and observed for fluorescence with the LSM system. The observed area in the striatum was similar to the imaged region in **Fig. 2C, D**. For quantitative evaluation, the number of TUNEL-positive cells was counted in 4 sections/rat. Five rats were used to obtain the quantitative data.

Histological analysis of neutrophil influx

Frozen sections (7 μm) were prepared as described above. For fixation of these sections, they were incubated in acetone for 1 min at room temperature, and then in 0.3% H_2O_2 solution for 30 min at room temperature. After having been blocked with fetal bovine serum for 20 min at room temperature, the sections were incubated with anti-myeloperoxidase (MPO) rabbit polyclonal antibody (Thermo Fisher Scientific, Rockford, IL, USA) for 30 min at room temperature. A Vectastain ABC rabbit IgG kit and DAB peroxidase substrate kit (both from Vector Laboratories, Inc., Burlingame, CA, USA) were used for identification of neutrophils in the sections. Finally, the sections were counterstained with hematoxylin and observed microscopically (BX51; Olympus, Tokyo, Japan). The observed area in the striatum was similar to the imaged region in Fig. 2*C, D*.

Therapeutic experiment

FK506-liposomes (30 or 100 μg/kg as FK506 dosage), PBS, free FK506 (30, 100, or 300 μg/kg), or vehicle (200 mg/ml HCO-60 including 10% ethanol in PBS) for FK506 were intravenously injected into t-MCAO rats immediately after the start of reperfusion. The volume of damaged region, the degree of brain swelling, and the functional outcome of rats were assessed at 24 h after the injection. For the functional outcome study, the rats underwent a 21-point neurological score analysis prior to sacrifice, as described previously (18). All of the normal and sham-operated rats received 21 points in this test. After this study, the brains of t-MCAO rats were sliced into 2-mm-thick coronal sections by using a rat brain slicer (Muromachi Kikai) and stained with 2,3,5-triphenyltetrazolium chloride (TTC; Wako) for the detection of cerebral cell death. The volume of the damaged regions was calculated by using an image-analysis system (Image J; U.S. National Institutes of Health, Bethesda, MD, USA). The damaged regions were considered to be those appearing completely white. Brain swelling was calculated as the ratio of volumes between ipsilateral and contralateral hemisphere sections.

Assessment of therapeutic time window

t-MCAO rats were intravenously injected with FK506-liposomes (30 or 100 μg/kg as FK506 dosage) or PBS at various times after the start of reperfusion. The volume of damaged regions was assessed at 24 h after injection by using TTC staining as described above.

Statistical analysis

Statistical analysis was performed by 1-way analysis of variance (ANOVA) followed by Dunnett's multiple comparison tests. Data are presented as means ± SD.

RESULTS

FK506-liposomes protected differentiated PC12 cells from H_2O_2-induced toxicity

The particle size and ζ-potential of FK506 liposomes were 109 ± 4.3 nm and −7.2 ± 0.7 mV, respectively. To

assess the pharmacological activity of FK506-liposomes, we examined the cytoprotective effect of them on differentiated PC12 cells treated with H_2O_2. The number of live PC12 cells was decreased to ~40% by exposure to H_2O_2 (**Fig. 1**). FK506-liposomes suppressed this cell death induced by H_2O_2 in a dose-dependent manner, whereas empty-liposomes (PEGylated liposomes) showed no cytoprotective effect against the H_2O_2-induced toxicity.

FK506-liposomes diffused into the brain parenchyma only in the ischemic hemisphere

The intracerebral distribution of FK506-liposomes given immediately after the start of reperfusion to t-MCAO rats was observed at 3 h (Fig. 2*A*) and 24 h (Fig. 2*B*) after the injection. The fluorescence of DiI-labeled FK506-liposomes was observed only in the ischemic hemisphere at both time points. Immunohistological analysis revealed that the FK506-liposomes had leaked into the brain parenchyma from cerebral vessels in the ipsilateral hemisphere (Fig. 2*C, D*). Moreover, higher DiI fluorescence intensity was detected in the brain sections prepared at 24 h after the injection than in those prepared at 3 h (Fig. 2*E*) after it, which suggests that the accumulation of FK506-liposomes in the brain parenchyma gradually increased by continuous leakage from cerebral vessels according to enhanced permeability and the retention effect. In contrast, no leakage of them into the cerebral parenchyma of the contralateral hemisphere occurred.

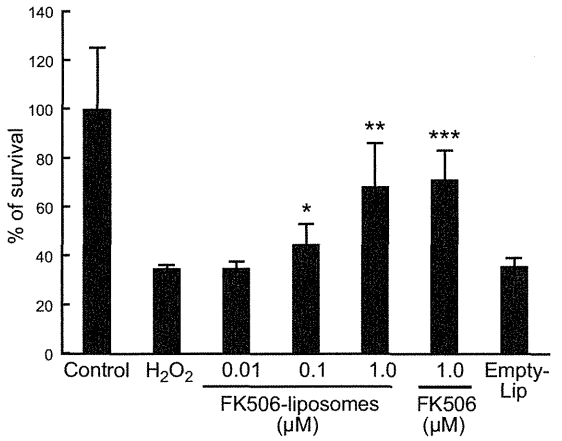

Figure 1. FK506-liposome-mediated attenuation of H_2O_2-induced cytotoxicity toward differentiated PC12 cells. PC12 cells were caused to differentiate by the addition of NGF at 100 ng/ml to culture medium supplemented with 0.5% HS. After 5 d in culture for differentiation, FK506-liposomes, free FK506, or empty liposomes (Empty-Lip) were added to the culture medium, and then H_2O_2 was added to each well. After 24 h, viable cell numbers were determined by performing the WST assay. Final lipid concentration of empty liposomes was same as that of FK506-liposomes. Data are presented as means ± SD (n=6). $^*P < 0.05$, $^{**}P < 0.01$, $^{***}P < 0.001$ *vs.* H_2O_2-treated group.

FK506-liposomes showed antiapoptotic effect in t-MCAO rats

At 24 h after the injection of each sample, apoptosis of the cerebral cells in t-MCAO rats was identified by TUNEL staining (**Fig. 3**). TUNEL-positive cells were detected in neither the striatum nor the cerebral cortex in the nonischemic hemisphere (data not shown). A number of apoptotic cells were observed in the control group and free FK506-treated group (Fig. 3*A, B*). This dosage (100 μg/kg) of free FK506 was too low to exert an antiapoptotic effect in t-MCAO rats. However, FK506-liposomes obviously reduced the number of TUNEL-positive cells despite the same dosage as free FK506. Quantitative analysis of TUNEL-positive cells elucidated the difference between each group (Fig. 3*C*). In the FK506-liposome-treated group, the number of apoptotic cells in the striatum was significantly reduced compared with that in the other groups. In contrast to this result, there was no significant difference in the cortex between FK506-liposome-treated group and other groups, even though this treatment tended to suppress the cerebral apoptosis. Empty liposomes had no effect on apoptosis induced by I/R injury.

FK506-liposomes suppressed neutrophil invasion induced by I/R

To evaluate anti-inflammatory effect of FK506-liposomes, we examined neutrophil invasion into I/R regions as an indicator of intracerebral inflammation (**Fig. 4**). In the nonischemic hemisphere of all groups, almost no MPO-stained cells were identified (data not shown). Conversely, a number of neutrophils that had infiltrated were detected in the striatum and the cortex of the ischemic hemisphere (Fig. 4*A*, control). In the FK506-liposome-treated group, few MPO-positive cells were observed in the striatum, whereas they were more numerous in the cortex. The quantitative analysis revealed that FK506-liposomes reduced the number of infiltrating neutrophils in the striatum by ~80%, and significantly suppressed neutrophil invasion compared with the treatment with the same dosage of free FK506 (Fig. 4*B*).

FK506-liposomes ameliorated cerebral I/R injury in t-MCAO rats

t-MCAO caused cerebral cell death and brain swelling in these experimental model rats. Treatment with free FK506 at 30 or 100 μg/kg hardly affected the damaged region and brain swelling induced by I/R, whereas FK506-liposomes at these same dosages as the free drug significantly reduced the amount of brain damage (**Fig. 5A, B**). Furthermore, administration of FK506-liposomes at 100 μg/kg showed therapeutic efficacy quite similar to that obtained with the free drug at 300 μg/kg. These results suggest that liposomalization of FK506 enhanced its cytoprotective

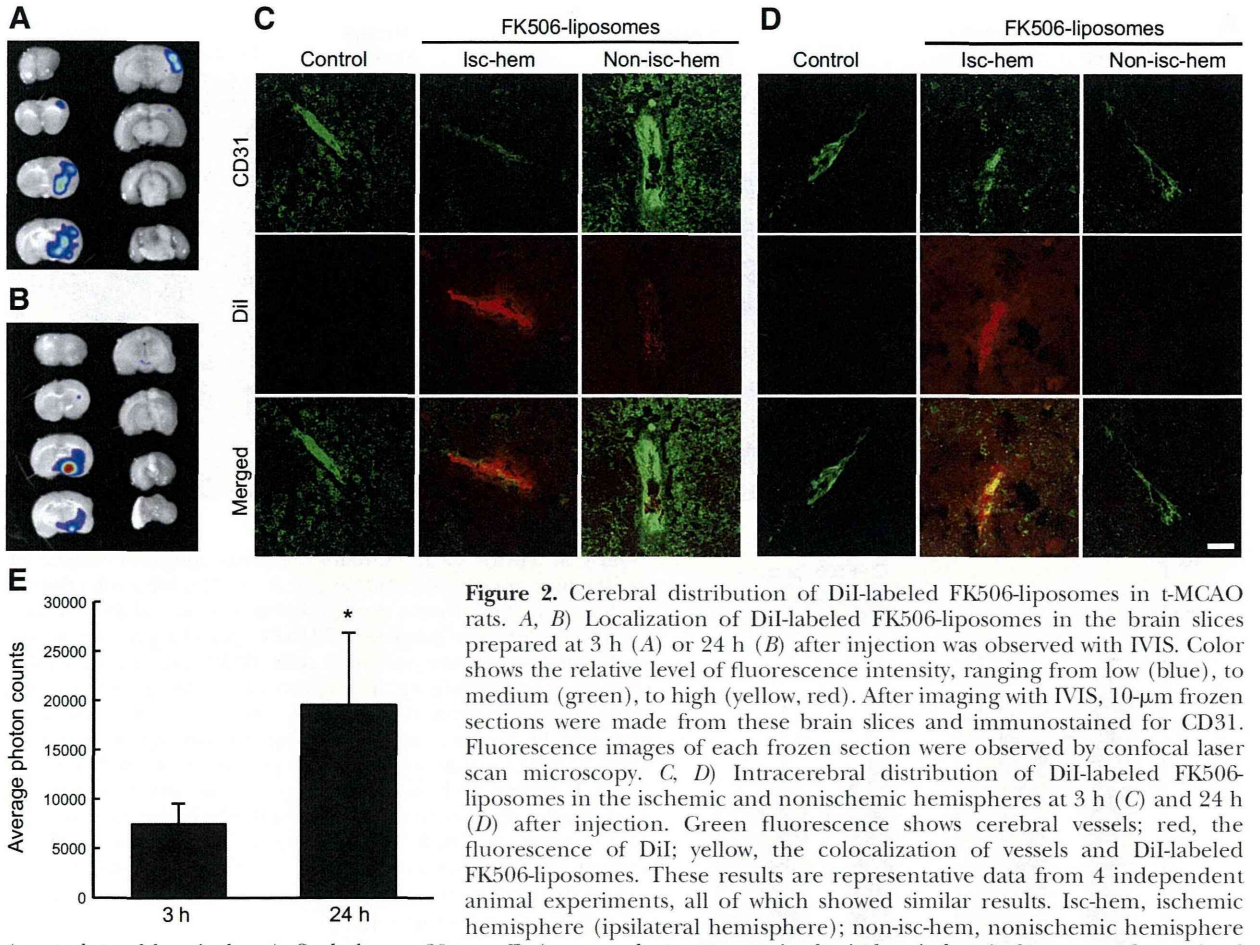

Figure 2. Cerebral distribution of DiI-labeled FK506-liposomes in t-MCAO rats. *A*, *B*) Localization of DiI-labeled FK506-liposomes in the brain slices prepared at 3 h (*A*) or 24 h (*B*) after injection was observed with IVIS. Color shows the relative level of fluorescence intensity, ranging from low (blue), to medium (green), to high (yellow, red). After imaging with IVIS, 10-μm frozen sections were made from these brain slices and immunostained for CD31. Fluorescence images of each frozen section were observed by confocal laser scan microscopy. *C*, *D*) Intracerebral distribution of DiI-labeled FK506-liposomes in the ischemic and nonischemic hemispheres at 3 h (*C*) and 24 h (*D*) after injection. Green fluorescence shows cerebral vessels; red, the fluorescence of DiI; yellow, the colocalization of vessels and DiI-labeled FK506-liposomes. These results are representative data from 4 independent animal experiments, all of which showed similar results. Isc-hem, ischemic hemisphere (ipsilateral hemisphere); non-isc-hem, nonischemic hemisphere (contralateral hemisphere). Scale bar = 20 μm. *E*) Average photon counts in the ischemic hemisphere were determined by the image of brain slices with IVIS (n=4). *$P < 0.05$.

effect due to improved biodistribution. In accordance with several reports, the extent of cerebral cell death, as indicated by reduced brain volume (Fig. 5*A*), and that of brain swelling (Fig. 5*B*) were similar in both control (PBS-injected) and vehicle-injected groups.

The therapeutic time window (TTW) of agents is critical information for developing neuroprotectants, particularly in designing the clinical trial. The TTW of FK506-liposomes was estimated by altering the time of injection after the commencement of reperfusion (Fig. 6). The volume of brain damage in the t-MCAO rats was significantly decreased by the dose of FK506-liposomes administered at 30 μg/kg as FK506 up through 2 h after reperfusion had begun. However, the treatment with the same dose of FK506-liposomes given at 3 h after the start of reperfusion or later had almost no effect on cerebral cell death, as judged by the results of TTC staining. Moreover, a higher amount of FK506-liposomes (100 μg/kg as FK506) injected at 3 h after reperfusion had begun also scarcely suppressed the brain damage. Taken together, these data indicate that the therapeutic time window for FK506-liposomes was up to 2 h after MCAO/reperfusion in this experimental model rat, and suggest that the injection of them at an early time would result in a good outcome.

The motor ability of the t-MCAO rats was evaluated based on the 21-point motor score (**Fig. 7**). In the control group, hemiparesis was observed at 24 h after the start of reperfusion, resulting in a low score. On the other hand, t-MCAO rats treated with FK506-liposomes showed alleviated hemiparesis, especially in their hind legs. This recovery probably contributed to the high scores on the inclined platform test, horizontal bar test (forepaws placed on ribbed bar), and circling test obtained for the FK506-liposome-treated animals (Supplemental Table S1). The administration of free FK506 at 300 μg/kg also significantly improved motor function deficit. These results correlated well with the extent of cerebral cell death and swelling.

DISCUSSION

The present study showed that FK506-liposomes significantly suppressed neutrophil invasion and apoptotic cell death, and ameliorated neurological deficits in t-MCAO rats compared with free FK506. The liposomalization of FK506 might lead to an increase in the amount of drug accumulation in I/R regions. The disruption of blood-brain barrier is induced at an early

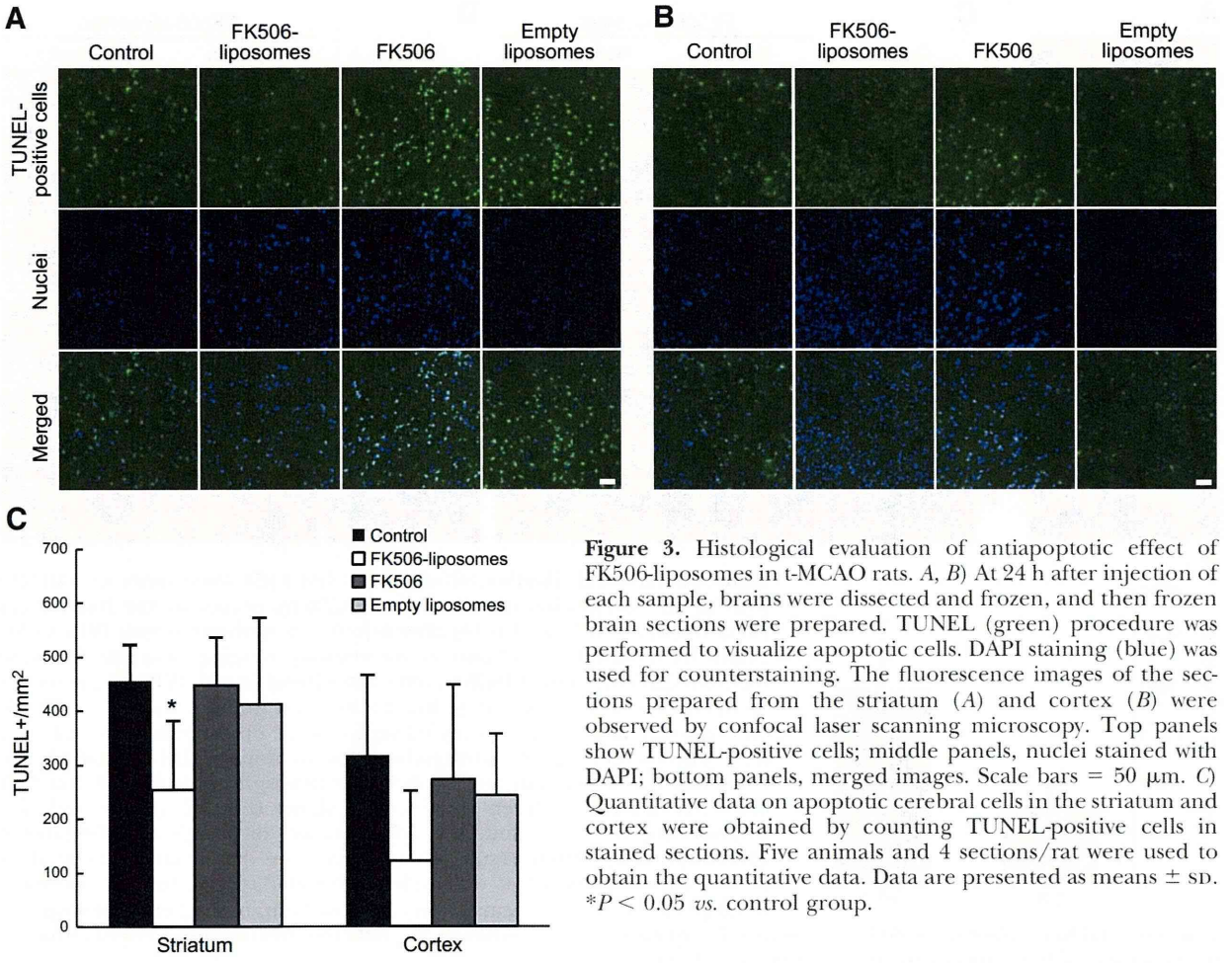

Figure 3. Histological evaluation of antiapoptotic effect of FK506-liposomes in t-MCAO rats. *A, B*) At 24 h after injection of each sample, brains were dissected and frozen, and then frozen brain sections were prepared. TUNEL (green) procedure was performed to visualize apoptotic cells. DAPI staining (blue) was used for counterstaining. The fluorescence images of the sections prepared from the striatum (*A*) and cortex (*B*) were observed by confocal laser scanning microscopy. Top panels show TUNEL-positive cells; middle panels, nuclei stained with DAPI; bottom panels, merged images. Scale bars = 50 μm. *C*) Quantitative data on apoptotic cerebral cells in the striatum and cortex were obtained by counting TUNEL-positive cells in stained sections. Five animals and 4 sections/rat were used to obtain the quantitative data. Data are presented as means ± SD. $^{*}P < 0.05$ *vs.* control group.

stage in the ischemic core region after cerebral ischemia (19, 20). Moreover, a previous report demonstrated that the area in which macromolecules accumulate expands as time passes after I/R in t-MCAO rats (21). Hence, the concept of passive targeting, as constructed for cancer treatment, could be a promising scheme for efficient drug delivery to I/R regions. In the present study, a higher extent of localization of FK506-liposomes in the ischemic hemisphere was observed at 24 h than at 3 h after the injection. This result suggests that the accumulation amount of FK506-liposomes given at the start of reperfusion gradually increased in

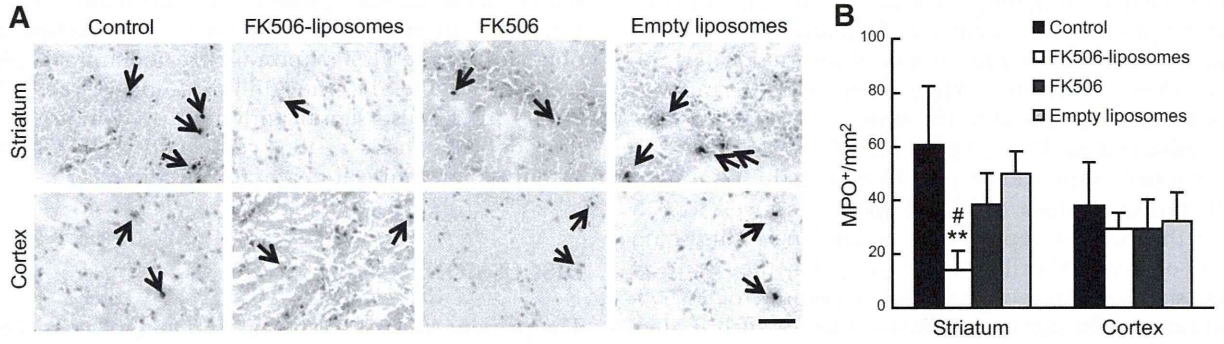

Figure 4. Invasion of neutrophils into the brain parenchyma of t-MCAO rats. At 24 h after injection of each sample, brains were dissected and frozen; and then frozen brain sections were prepared. MPO immunostaining was performed to visualize neutrophils (brown). Hematoxylin staining (blue) was used for counterstaining. *A*) Stained sections were observed by microscopy. Arrows indicate neutrophils that had infiltrated the brain parenchyma. Scale bar = 50 μm. *B*) Quantitative data on neutrophil invasion analysis were obtained by counting MPO-positive cells in stained sections. Data are presented as means ± SD (n=6). $^{**}P < 0.01$ *vs.* control group; $^{\#}P < 0.05$ *vs.* free FK506-treated group.

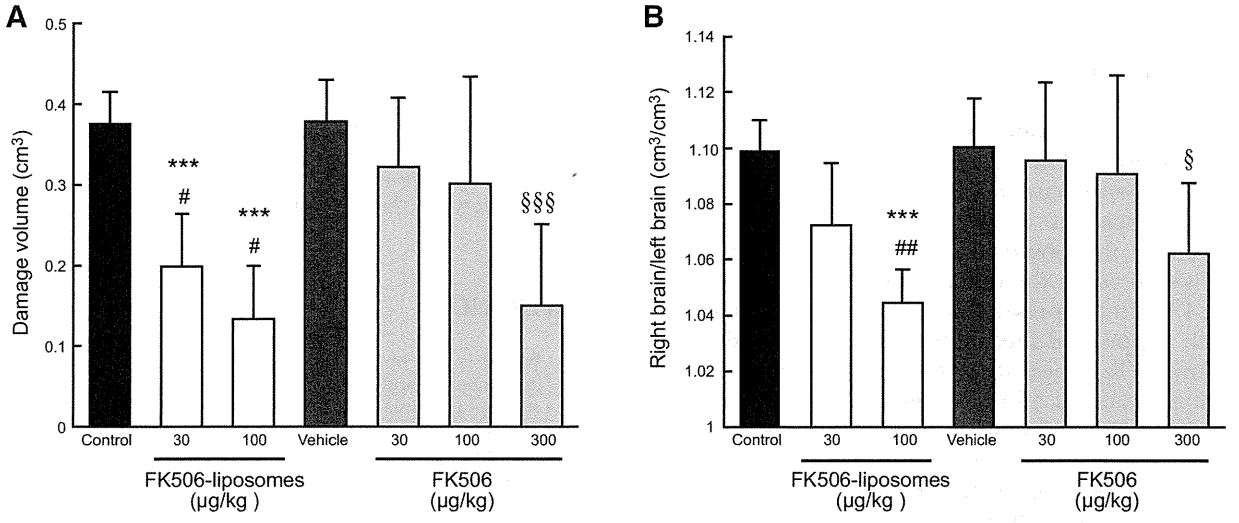

Figure 5. Suppression of cerebral cell death and brain swelling by the treatment with FK506-liposomes. t-MCAO rats were injected *via* a tail vein with PBS, FK506-liposomes, vehicle for free FK506 or free FK506 immediately after the start of reperfusion at dosages indicated as FK506. At 24 h after injection, brains were dissected and stained with TTC. Damage volume (*A*) and degree of brain swelling (*B*) were calculated by using Image J. Data are means ± SD (n=7). $^{***}P < 0.001$ *vs.* control group; $^{\#}P < 0.05$, $^{\#\#}P < 0.01$ *vs.* free FK506-treated group at the same dose; $^{\S}P < 0.05$, $^{\S\S\S}P < 0.001$ *vs.* vehicle-treated group.

a time-dependent manner, as in the case of enhanced permeability and retention effect. However, the half-life of free FK506 is extremely short, and FK506 administered intravenously is almost totally metabolized by the liver, primarily by cytochrome P450 3A (22, 23). The change in biodistribution afforded by liposomalization would be expected to be closely related to the therapeutic outcome.

Fatal damage in the striatum, the region assumed to be the ischemic core in the present experimental model, occurs at an early stage after an I/R event (21). In this study, FK506-liposomes substantially reduced the cerebral cell death and inflammation induced by I/R in this region. Thus, FK506-liposomes spreading into the brain parenchyma quickly showed pharmacological activity. Although PEG-modification of liposomes prolongs their circulation in the blood, it causes a decrease in cellular uptake of liposomes (24, 25). Therefore, FK506-liposomes reaching I/R regions might have released FK506 into the brain parenchyma, and the released drugs then acted on the cerebral cells.

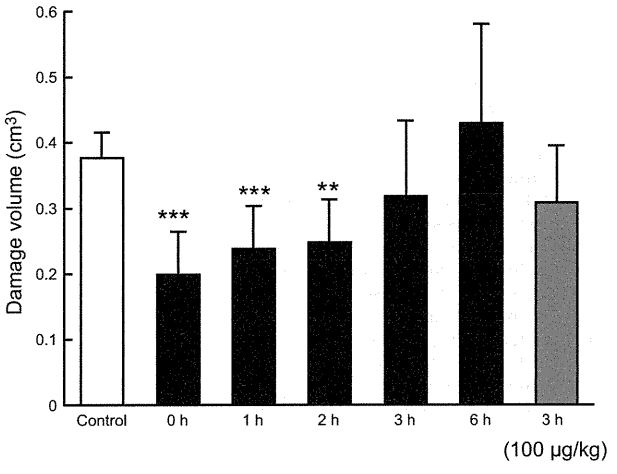

Figure 6. Therapeutic time window of FK506-liposomes in t-MCAO rats. t-MCAO rats were intravenously injected *via* a tail vein with FK506-liposomes (30 or 100 μg/kg as FK506 dosage) at the indicated times (0, 1, 2, 3, or 6 h) after the start of reperfusion. At 24 h after reperfusion had begun, brain was dissected and stained with TTC. Damage volume was calculated by using Image J. Data are presented as means ± SD (n=6–7). $^{**}P < 0.01$, $^{***}P < 0.001$ *vs.* control.

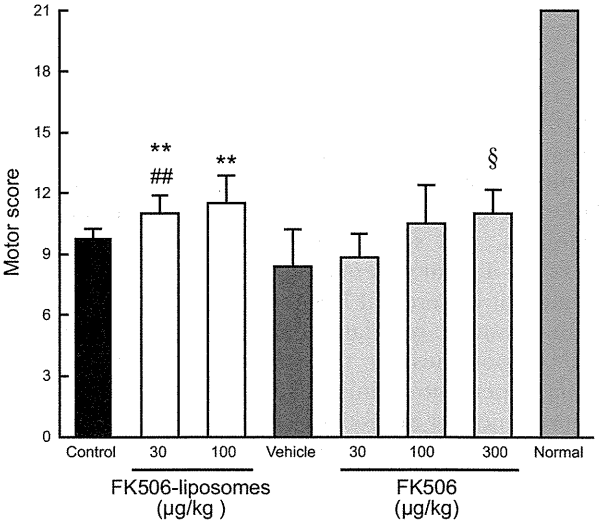

Figure 7. Motor activity score of t-MCAO rats. t-MCAO rats were treated with each sample as described in the legend of Fig. 5, and these rats were then assessed for motor function in a 21-point neuropathological scoring system. Data are presented as means ± SD (n=7). $^{**}P < 0.01$ *vs.* control group; $^{\#\#}P < 0.01$ *vs.* free FK506-treated group at the same dose; $^{\S}P < 0.05$ *vs.* vehicle-treated group.

Neutrophils generate cytotoxic substances such as hypochlorous acid in inflammation sites, resulting in progressive inflammation. These cells normally do not exist in the brain, but they do invade into the cerebral parenchyma *via* brain endothelial cells after a cerebral ischemic event. This invasion induced by intracerebral inflammation occurs during the period of 9 to 24 h after the start of reperfusion in t-MCAO rats (26). Therefore, the observation of neutrophil invasion is one way to assess the extent of cerebral inflammation after I/R. In the present study, FK506-liposomes significantly suppressed the neutrophil invasion induced by cerebral I/R. A past study showed that FK506 inhibits the expression of adhesion molecules in the cerebral vasculature by reducing the production of inflammatory cytokines by neuronal cells and glia cells (26). Accordingly, we suggest that FK506-liposomes administered after the start of reperfusion inhibited the inflammatory response by affecting neuronal cells and glia cells in the t-MCAO rats.

FK506 directly suppresses apoptotic cell death induced by cerebral I/R through the inhibition of Bad dephosphorylation and subsequent cytochrome *c* release (27, 28). In addition, the prevention of reactive oxygen species production is related to its antiapoptotic effect on cerebral cells injured by I/R (29). The present study demonstrated that FK506-liposomes markedly reduced the number of apoptotic cells in t-MCAO rats. These multifunctional mechanisms, including the anti-inflammatory effect of FK506-liposomes, probably effectively acted on the neurovascular unit to bring about the good outcome in the t-MCAO rats.

A large number of small molecules as neuroprotectants have failed in clinical trials (30). Based on our present data, we propose that liposomalization of small molecular neuroprotectants should overcome their insufficiency of medicinal efficacy and adverse side effects. Liposomes can encapsulate many kinds of drugs regardless of their being hydrophilic or hydrophobic. Furthermore, liposomes can be modified with functional molecules, resulting in improved biodistribution, controlled release of drugs, increase in drug accumulation in targeted cells, regulation of intracellular distribution, and so on (31–34). Therefore, liposomal DDS has a great potential to be a novel strategy for the treatment of cerebral I/R injury.

In summary, our data demonstrate the usefulness of FK506-liposomes for the treatment of cerebral ischemia/reperfusion injury. FK506-liposomes intravenously injected immediately after the start of reperfusion significantly suppressed neutrophil invasion, apoptotic cell death, and infarct volume compared with free FK506 in t-MCAO rats. In addition, the motor function deficits induced by ischemia/reperfusion in these rats were ameliorated to a greater extent by the treatment with FK506-liposomes than by that with free FK506. Therefore, liposomalization of FK506 should permit a reduction in the dosage of FK506 without a decrease in the therapeutic efficacy of the drug. Taken together, our present findings indicate that FK506-liposomes have a clear potential to be a neuroprotectant if administered quickly after a cerebral stroke. FJ

The authors thank Astellas Pharmaceutical Co., Ltd. (Tokyo, Japan) for the gift of the FK506. This research was supported by a grant-in-aid for scientific research from the Japan Society for the Promotion of Science.

REFERENCES

1. Wong, C. H., and Crack, P. J. (2008) Modulation of neuroinflammation and vascular response by oxidative stress following cerebral ischemia-reperfusion injury. *Curr. Med. Chem.* **15,** 1–14
2. Eltzschig, H. K., and Eckle, T. (2011) Ischemia and reperfusion–from mechanism to translation. *Nat. Med.* **17,** 1391–1401
3. Tuma, R. F., and Steffens, S. (2012) Targeting the endocannabinod system to limit myocardial and cerebral ischemic and reperfusion injury. *Curr. Pharm. Biotechnol.* **13,** 46–58
4. Ginsberg, M. D. (2009) Current status of neuroprotection for cerebral ischemia: synoptic overview. *Stroke* **40,** S111–114
5. Ishii, T., Asai, T., Oyama, D., Fukuta, T., Yasuda, N., Shimizu, K., Minamino, T., and Oku, N. (2012) Amelioration of cerebral ischemia-reperfusion injury based on liposomal drug delivery system with asialo-erythropoietin. *J. Control. Release* **160,** 81–87
6. Sharkey, J., and Butcher, S. P. (1994) Immunophilins mediate the neuroprotective effects of FK506 in focal cerebral ischaemia. *Nature* **371,** 336–339
7. Furuichi, Y., Maeda, M., Moriguchi, A., Sawamoto, T., Kawamura, A., Matsuoka, N., Mutoh, S., and Yanagihara, T. (2003) Tacrolimus, a potential neuroprotective agent, ameliorates ischemic brain damage and neurologic deficits after focal cerebral ischemia in nonhuman primates. *J. Cereb. Blood Flow Metab.* **23,** 1183–1194
8. Szydlowska, K., Zawadzka, M., and Kaminska, B. (2006) Neuroprotectant FK506 inhibits glutamate-induced apoptosis of astrocytes in vitro and in vivo. *J. Neurochem.* **99,** 965–975
9. Morioka, M., Hamada, J., Ushio, Y., and Miyamoto, E. (1999) Potential role of calcineurin for brain ischemia and traumatic injury. *Prog. Neurobiol.* **58,** 1–30
10. Wang, H. G., Pathan, N., Ethell, I. M., Krajewski, S., Yamaguchi, Y., Shibasaki, F., McKeon, F., Bobo, T., Franke, T. F., and Reed, J. C. (1999) Ca2+-induced apoptosis through calcineurin dephosphorylation of BAD. *Science* **284,** 339–343
11. Hashiguchi, A., Kawano, T., Yano, S., Morioka, M., Hamada, J., Sato, T., Shirasaki, Y., Ushio, Y., and Fukunaga, K. (2003) The neuroprotective effect of a novel calmodulin antagonist, 3-[2-[4-(3-chloro-2-methylphenyl)-1-piperazinyl]ethyl]-5,6-dimethoxy-1-(4-imidazolylmethyl)-1H-indazole dihydrochloride 3.5 hydrate, in transient forebrain ischemia. *Neuroscience* **121,** 379–386
12. Kaminska, B., Gaweda-Walerych, K., and Zawadzka, M. (2004) Molecular mechanisms of neuroprotective action of immunosuppressants–facts and hypotheses. *J. Cell. Mol. Med.* **8,** 45–58
13. Chuang, Y. C., Tyagi, P., Huang, H. Y., Yoshimura, N., Wu, M., Kaufman, J., and Chancellor, M. B. (2011) Intravesical immune suppression by liposomal tacrolimus in cyclophosphamide-induced inflammatory cystitis. *Neurourol. Urodyn.* **30,** 421–427
14. Moffatt, S. D., McAlister, V., Calne, R. Y., and Metcalfe, S. M. (1999) Potential for improved therapeutic index of FK506 in liposomal formulation demonstrated in a mouse cardiac allograft model. *Transplantation* **67,** 1205–1208
15. Longa, E. Z., Weinstein, P. R., Carlson, S., and Cummins, R. (1989) Reversible middle cerebral artery occlusion without craniectomy in rats. *Stroke* **20,** 84–91
16. Zhang, N., Komine-Kobayashi, M., Tanaka, R., Liu, M., Mizuno, Y., and Urabe, T. (2005) Edaravone reduces early accumulation of oxidative products and sequential inflammatory responses after transient focal ischemia in mice brain. *Stroke* **36,** 2220–2225
17. Toung, T. J., Bhardwaj, A., Dawson, V. L., Dawson, T. M., Traystman, R. J., and Hurn, P. D. (1999) Neuroprotective FK506 does not alter in vivo nitric oxide production during ischemia and early reperfusion in rats. *Stroke* **30,** 1279–1285

18. Hunter, A. J., Hatcher, J., Virley, D., Nelson, P., Irving, E., Hadingham, S. J., and Parsons, A. A. (2000) Functional assessments in mice and rats after focal stroke. *Neuropharmacology* **39,** 806–816
19. Rosenberg, G. A., Estrada, E. Y., and Dencoff, J. E. (1998) Matrix metalloproteinases and TIMPs are associated with blood-brain barrier opening after reperfusion in rat brain. *Stroke* **29,** 2189–2195
20. Dirnagl, U., Iadecola, C., and Moskowitz, M. A. (1999) Pathobiology of ischaemic stroke: an integrated view. *Trends Neurosci.* **22,** 391–397
21. Ishii, T., Asai, T., Urakami, T., and Oku, N. (2010) Accumulation of macromolecules in brain parenchyma in acute phase of cerebral infarction/reperfusion. *Brain Res.* **1321,** 164–168
22. Yura, H., Yoshimura, N., Hamashima, T., Akamatsu, K., Nishikawa, M., Takakura, Y., and Hashida, M. (1999) Synthesis and pharmacokinetics of a novel macromolecular prodrug of Tacrolimus (FK506), FK506-dextran conjugate. *J. Control. Release* **57,** 87–99
23. Shiraga, T., Matsuda, H., Nagase, K., Iwasaki, K., Noda, K., Yamazaki, H., Shimada, T., and Funae, Y. (1994) Metabolism of FK506, a potent immunosuppressive agent, by cytochrome P450 3A enzymes in rat, dog and human liver microsomes. *Biochem. Pharmacol.* **47,** 727–735
24. Duzgune, scedil, and Nir, S. (1999) Mechanisms and kinetics of liposome-cell interactions. *Adv. Drug Deliv. Rev.* **40,** 3–18
25. Vertut-Doi, A., Ishiwata, H., and Miyajima, K. (1996) Binding and uptake of liposomes containing a poly(ethylene glycol) derivative of cholesterol (stealth liposomes) by the macrophage cell line J774: influence of PEG content and its molecular weight. *Biochim. Biophys. Acta* **1278,** 19–28
26. Noto, T., Furuichi, Y., Ishiye, M., Matsuoka, N., Aramori, I., Mutoh, S., and Yanagihara, T. (2007) Tacrolimus (FK506) limits accumulation of granulocytes and platelets and protects against brain damage after transient focal cerebral ischemia in rat. *Biol. Pharm. Bull.* **30,** 313–317
27. Li, J. Y., Furuichi, Y., Matsuoka, N., Mutoh, S., and Yanagihara, T. (2006) Tacrolimus (FK506) attenuates biphasic cytochrome c release and Bad phosphorylation following transient cerebral ischemia in mice. *Neuroscience* **142,** 789–797
28. Shichinohe, H., Kuroda, S., Abumiya, T., Ikeda, J., Kobayashi, T., Yoshimoto, T., and Iwasaki, Y. (2004) FK506 reduces infarct volume due to permanent focal cerebral ischemia by maintaining BAD turnover and inhibiting cytochrome c release. *Brain Res.* **1001,** 51–59
29. Dawson, T. M., Steiner, J. P., Dawson, V. L., Dinerman, J. L., Uhl, G. R., and Snyder, S. H. (1993) Immunosuppressant FK506 enhances phosphorylation of nitric oxide synthase and protects against glutamate neurotoxicity. *Proc. Natl. Acad. Sci. U.¦S.¦A.* **90,** 9808–9812
30. Sahota, P., and Savitz, S. I. (2011) Investigational therapies for ischemic stroke: neuroprotection and neurorecovery. *Neurotherapeutics* **8,** 434–451
31. Asai, T., Matsushita, S., Kenjo, E., Tsuzuku, T., Yonenaga, N., Koide, H., Hatanaka, K., Dewa, T., Nango, M., Maeda, N., Kikuchi, H., and Oku, N. (2011) Dicetyl phosphate-tetraethylenepentamine-based liposomes for systemic siRNA delivery. *Bioconjug. Chem.* **22,** 429–435
32. Tan, M. L., Choong, P. F., and Dass, C. R. (2010) Recent developments in liposomes, microparticles and nanoparticles for protein and peptide drug delivery. *Peptides* **31,** 184–193
33. Torres, E., Mainini, F., Napolitano, R., Fedeli, F., Cavalli, R., Aime, S., and Terreno, E. (2011) Improved paramagnetic liposomes for MRI visualization of pH triggered release. *J. Control. Release* **154,** 196–202
34. Micheli, M. R., Bova, R., Magini, A., Polidoro, M., and Emiliani, C. (2012) Lipid-based nanocarriers for CNS-targeted drug delivery. *Recent Pat. CNS Drug Discov.* **7,** 71–86

Received for publication October 1, 2012.
Accepted for publication December 4, 2012.

Cardiovasc Drugs Ther (2013) 27:125–132
DOI 10.1007/s10557-012-6437-6

ORIGINAL ARTICLE

Liposomal Amiodarone Augments Anti-arrhythmic Effects and Reduces Hemodynamic Adverse Effects in an Ischemia/Reperfusion Rat Model

Hiroyuki Takahama · Hirokazu Shigematsu · Tomohiro Asai · Takashi Matsuzaki · Shoji Sanada · Hai Ying Fu · Keiji Okuda · Masaki Yamato · Hiroshi Asanuma · Yoshihiro Asano · Masanori Asakura · Naoto Oku · Issei Komuro · Masafumi Kitakaze · Tetsuo Minamino

Published online: 24 January 2013

Abstract
Purpose Although amiodarone is recognized as the most effective anti-arrhythmic drug available, it has negative hemodynamic effects. Nano-sized liposomes can accumulate in and selectively deliver drugs to ischemic/reperfused (I/R) myocardium, which may augment drug effects and reduce side effects. We investigated the effects of liposomal amiodarone on lethal arrhythmias and hemodynamic parameters in an ischemia/reperfusion rat model.
Methods and Results We prepared liposomal amiodarone (mean diameter: 113±8 nm) by a thin-film method. The left coronary artery of experimental rats was occluded for 5 min followed by reperfusion. Ex vivo fluorescent imaging revealed that intravenously administered fluorescent-labeled nano-sized beads accumulated in the I/R myocardium. Amiodarone was measurable in samples from the I/R myocardium when liposomal amiodarone, but not amiodarone, was administered. Although the intravenous administration of amiodarone (3 mg/kg) or liposomal amiodarone (3 mg/kg) reduced heart rate and systolic blood pressure compared with saline, the decrease in heart rate or systolic blood pressure caused by liposomal amiodarone was smaller compared with a corresponding dose of free amiodarone. The intravenous administration of liposomal amiodarone (3 mg/kg), but not free amiodarone (3 mg/kg), 5 min before ischemia showed a significantly reduced duration of lethal arrhythmias (18±9 s) and mortality (0 %) during the reperfusion period compared with saline (195±42 s, 71 %, respectively).
Conclusions Targeting the delivery of liposomal amiodarone to ischemic/reperfused myocardium reduces the mortality due to lethal arrhythmia and the negative hemodynamic changes caused by amiodarone. Nano-size liposomes may be a promising drug delivery system for targeting I/R myocardium with cardioprotective agents.

Keywords Liposome · Amiodarone · Lethal arrhythmia · Ischemia · Reperfusion

T. Matsuzaki · S. Sanada · H. Y. Fu · K. Okuda · M. Yamato · Y. Asano · I. Komuro · T. Minamino (✉)
Department of Cardiovascular Medicine, Osaka University Graduate School of Medicine, 2-2 Yamadaoka, Suita, Osaka 565-0871, Japan
e-mail: minamino@cardiology.med.osaka-u.ac.jp

H. Takahama · M. Asakura · M. Kitakaze
Department of Cardiovascular Medicine, National Cerebral and Cardiovascular Center, Suita 565-8565, Japan

H. Shigematsu · T. Asai · N. Oku
Department of Medical Biochemistry and Global COE, University of Shizuoka Graduate School of Pharmaceutical Sciences, Shizuoka 422-8526 Shizuoka, Japan

H. Asanuma
Department of Cardiovascular Science and Technology, Kyoto Prefectural University School of Medicine, Kyoto 602-8566, Japan

H. Takahama
Division of Cardiovascular Disease, Mayo Clinic, Rochester, MN 55902, USA

Introduction

Therapies for the prevention and treatment of ischemia-induced life-threatening arrhythmias remain an unmet medical need [1]. Amiodarone is currently considered to be the most effective anti-arrhythmic drug available for treating life-threatening arrhythmias [2, 3], despite the fact that this compound has a negative impact on hemodynamic parameters [4, 5]. The intravenous administration of amiodarone is expected

to be beneficial for the immediate treatment of arrhythmias in emergency settings, such as acute myocardial infarction (AMI) [6, 7]. However, in clinical practice, the administration of amiodarone remains problematic for the treatment of AMI [8]. Although lower doses of amiodarone result in fewer incidences of death, high doses of amiodarone can cause hypotension and non-cardiac death, both of which may diminish the positive effects of amiodarone [8, 9]. Therefore, a novel delivery system is strongly desired to enhance the anti-arrhythmic effects of amiodarone without producing severe side effects.

Liposomes are widely used for drug delivery to actively or passively target specific organs and to improve drug stability in cancer and inflammatory diseases [10–12]. In ischemic/reperfused (I/R) myocardium, cellular permeability is enhanced and vascular endothelial integrity is disrupted [13, 14], suggesting that nanoparticles, such as liposomes, may be a promising drug delivery system for targeting I/R myocardium with cardioprotective agents [15]. Indeed, we have recently demonstrated that adenosine encapsulated by liposomes coated with polyethylene glycol (PEG) exhibited enhanced cardioprotective effects and attenuated side effects, such as hypotension and bradycardia, in an ischemia/reperfusion model of rats [16]. In the present study, we prepared liposomal amiodarone and examined 1) the targeted accumulation of liposomal amiodarone in the I/R myocardium, 2) the hemodynamic effects of the intravenous administration of liposomal amiodarone and free amiodarone, and 3) the anti-arrhythmic effects of these preparations in an I/R rat model. We showed that targeting the delivery of liposomal amiodarone to I/R myocardium reduces the mortality due to lethal arrhythmias and the negative hemodynamic changes caused by amiodarone in an I/R rat model.

Methods

Materials

The materials used to prepare PEGylated liposomes, including 1-palmitoyl-2-oleoyl-sn-glycero-3-phosphocholine (POPC), 1,2-dipalmitoyl-sn-glycero-3-phosphocholine (DPPC), cholesterol, and 1,2-distearoyl-sn-glycero-3-phosphoethanolamine-N-poly(ethylene glycol) 2000 (DSPE-PEG2000), were kindly donated by Nippon Fine Chemical Co. (Takasago, Hyogo, Japan). Fluorescent beads (diameter 100 nm) were purchased from Invitrogen. All other materials were obtained from Sigma-Aldrich (St. Louis, MO, USA).

Animals

Male Wistar rats (9 weeks old and weighing 250–310 g; Japan Animals, Osaka, Japan) were used. The animal experiments were approved by the Osaka University Research Committee and were performed according to institutional guidelines. All studies conformed to the Guide for the care and Use of Laboratory Animals published by the US National Institutes of Health (NIH Publication No. 85–23, revised 1996).

Preparation of PEGylated Liposomes

PEGylated liposomes composed of POPC, DPPC, cholesterol, DSPE-PEG2000, and amiodarone were prepared by a thin-film method. Briefly, amiodarone and lipids dissolved in chloroform were evaporated to form a thin lipid film using a rotary evaporator. The lipid film was dried for at least 1 h under reduced pressure and then hydrated with PBS (pH7.4). The liposome solution was freeze-thawed for 3 cycles with liquid nitrogen. The particle size of the liposomes was adjusted by extrusion through 100-nm-pore polycarbonate filters (Nuclepore, Cambridge, MA, USA). The liposomal solutions were centrifuged at 453,000 g for 15 min (CS120GXL, Hitachi, Japan) to remove the untrapped amiodarone. Then, the liposomes were resuspended in PBS. To determine the efficacy of trapping amiodarone in the liposomes, an aliquot of the liposomal solution was solubilized with 1 % reduced Triton X-100 (Sigma-Aldrich), and the amount of amiodarone was optically determined at 240 nm.

Characterization of PEGylated Liposomes

The particle size and ζ potential of PEGylated liposomes diluted with PBS were measured by dynamic scatter analysis (Zetasizer Nano ZS; Malvern, Worcestershire, UK). The analyses were performed 15 times per sample, and the results represent the analysis of 3 independent experiments.

Experimental Protocol

Targeted Delivery of Fluorescent-labeled Nano-sized Beads to the I/R Myocardium

The rats were anesthetized with intraperitoneal sodium pentobarbital (50 mg/kg). Catheters were advanced into the femoral vein to infuse the drugs. Ischemia/reperfusion was induced by 5 min of left coronary artery occlusion followed by reperfusion [16]. After the hemodynamic parameters became stable, fluorescent-labeled nano-size beads, 100 nm in diameter (FluoSpheres, Invitrogen), were intravenously infused to the rats for 5 min before ischemia or before a sham operation (n=3, each). Fifteen minutes after reperfusion, the hearts were removed and cut into 5 sections parallel to the axis from the base to the apex. Then, ex vivo fluorescence images were obtained with an Olympus SZX12 stereoscopic microscope equipped with a DP71 digital camera (Olympus, Tokyo, Japan) before and after the hearts were sliced.

Targeted Delivery of Amiodarone and Liposomal Amiodarone to the I/R Myocardium

Catheters were advanced into the femoral artery and vein to measure the systemic blood pressure (BP) and to infuse the drugs into the anesthetized rats, respectively. Electrocardiographic and hemodynamic parameters, such as heart rate (HR) and BP, were continuously monitored during the study using a PowerLab system (ADInstruments, Castle Hill, Australia). After the hemodynamic parameters became stable, to clarify the targeted delivery of amiodarone and liposomal amiodarone to the I/R myocardium, we intravenously administered saline, free amiodarone (3 mg/kg) or liposomal amiodarone (3 mg/kg) to rats for 5 min before the onset of ischemia. Then, we obtained blood samples and myocardium from the I/R area.

Effects of Amiodarone and Liposomal Amiodarone on Lethal Arrhythmias

To evaluate the effects of amiodarone and liposomal amiodarone on lethal arrhythmias, we intravenously administered saline (n=7), free amiodarone (3.0 or 10.0 mg/kg) (n=6 each), PEGylated liposomes (empty liposomes) (n=6), and PEGylated liposomal amiodarone (3.0 mg/kg) (n=6) for 5 min before ischemia. The dose of amiodarone used in this study was lower than that used in a previous study [17] to clarify whether amiodarone encapsulated by liposomes coated with PEG exhibited enhanced anti-arrhythmic effects. Without any procedure such as electrical conversion or cardiac massage, ventricular tachyarrhythmias (VT/VF) occurred frequently during early period of reperfusion and the mortality of rats reached more than a half of cases in this model [18].

Measurement of Amiodarone Concentration

The concentration of amiodarone in serum and heart tissue from the I/R area was assayed by high-performance liquid chromatography (HPLC) as previously described [19]. The detection limit of the HPLC assay was 50 ng/mL. Blood and myocardial samples were obtained at the end of the experimental protocol. The sample preparation was performed as previously described [19]. Briefly, myocardium was freed from visible blood, thereafter rinsed with 0.9 % sodium chloride and stored at −20 °C until analysis. After that, myocardial tissue samples were finely minced and 100 mg were homogenized with 0.9 % sodium chloride (1 mL) and after centrifugation, the clear supernatant was injected into HPLC.

Quantitative Evaluation of Fluorescent-labeled Nano-sized Beads in the I/R Myocardium

To analyze the quantitative fluorescent intensity, signals from heart slices were quantified by image analysis (Image J; National Institutes of Health, USA) as previously described [20]. The signal intensity from the heart slices was evaluated as the average signals of the whole heart and the left ventricle (LV) (Fig. 2c).

Arrhythmia Analysis

The electrocardiographic tracings were independently analyzed by two of the authors, who were blinded to the treatment assignment. The duration of each spontaneous ventricular tachycardia or fibrillation episode during the I/R protocol was measured using the time scale provided by the recording software. Ventricular tachycardia was defined as 4 or more consecutive ventricular ectopic beats, and ventricular fibrillation was defined as a signal in which the individual QRS deflections could not easily be distinguished from one another. However, distinguishing ventricular tachycardia from fibrillation was often difficult [21]; therefore, we report ventricular tachycardia and fibrillation collectively as ventricular tachyarrhythmias (VT/VF) in this study. VT/VF duration and mortality were evaluated for 5 min of ischemia followed by 15 min of reperfusion.

Statistical Analysis

The parameters of the liposomes are expressed as the mean ± standard deviation (SD). Other data are expressed as the average ± standard error of the mean (SEM). To compare the parameters of the liposomes, unpaired t-tests were performed. We performed the Welch t-test to compare the amiodarone concentration in the plasma and myocardium. For hemodynamic parameters, the data were assessed with the paired t-test for comparisons to the baseline within a group. One-way repeated-measurement ANOVA followed by post-hoc Bonferroni's multiple comparisons were used for comparisons between groups. To address the differences in VT/VF duration among the groups, we performed a non-parametric (Kruskal-Wallis) test followed by evaluation with the Mann–Whitney U test. The mortality rates were compared using the Fisher's exact probability test. In all analyses, $P<0.05$ was considered to be statistically significant.

Results

Characterization of PEGylated Liposomes

We prepared 5 types of PEGylated liposomes composed of POPC, DPPC, cholesterol, and amiodarone. The ratio of unsaturated lipids (POPC) to saturated lipids (DPPC) varied (Fig. 1). During preparation of the liposomes, the POPC: DPPC:cholesterol:amiodarone molar ratio of 10:0:5:1 exhibited the best encapsulation efficiency for amiodarone compared with the other conditions (Fig. 1).

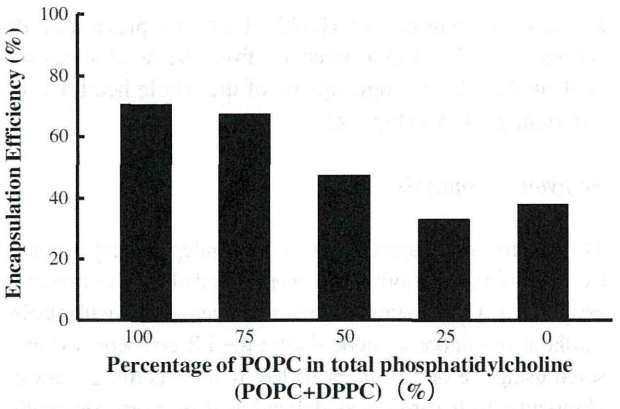

Fig. 1 Encapsulation efficiency of amiodarone in the liposomes. Amiodarone was loaded into liposomes containing POPC, DPPC, or a mixture of POPC and DPPC. The liposomal amiodarone was composed of phosphatidylcholine (POPC + DPPC):cholesterol:amiodarone at a 10:5:1 molar ratio. The percent molar ratio of POPC in total phosphatidylcholine (POPC + DPPC) is indicated in the figure. The encapsulation efficiency of amiodarone was determined as described in the Methods section

The dynamic light scatter analysis showed no significant differences between the mean diameter, polydispersity index, or ζ potential distribution of the empty and amiodarone-loaded PEGylated liposomes (Table 1).

Accumulation of Fluorescence-labeled Nano-sized Beads in the I/R Myocardium

Representative pictures obtained by fluorescence imaging are shown in Fig. 2a (whole heart) and b (sliced hearts). Quantitative analysis revealed that the average fluorescence intensity of the whole heart (Fig. 2c left) or the left ventricle (Fig. 2c right) of the I/R hearts was significantly higher than that in sham-operated hearts.

Amiodarone Concentration in the Blood and I/R Myocardium

The plasma concentration after the administration of liposomal amiodarone was significantly higher than that of free amiodarone (Table 2). Importantly, the amiodarone concentration in the I/R myocardium was detectable after the administration of liposomal, but not free, amiodarone (Table 2).

Hemodynamic Effects of Amiodarone and Liposomal Amiodarone

The baseline heart rates were 411±16, 426±14, 427±12, 409±8 and 414±6 beats/min in the saline, empty liposome, amiodarone (3 mg/kg), amiodarone (10 mg/kg) and liposomal amiodarone (3 mg/kg) groups, respectively. The baseline systolic BP was 113±7, 118±10, 111±5, 90±4 and 104±2 mmHg in the saline, empty liposome, amiodarone (3 mg/kg), amiodarone (10 mg/kg) and liposomal amiodarone (3 mg/kg) groups, respectively. There were no significant differences in the baseline HR or systolic BP among the groups tested. The intravenous administration of amiodarone (3 and 10 mg/kg) or liposomal amiodarone reduced both the HR and systolic BP from the baseline, whereas the saline or empty liposomes did not (Fig. 3). The time-course changes of both the HR and systolic BP were significantly smaller in the liposomal amiodarone group (3 mg/kg) compared with the corresponding dose in the free amiodarone group (3 mg/kg) (Fig. 3). The reductions in HR and systolic BP at 1, but not 3, minutes after liposomal amiodarone administration were significantly smaller compared with those following the corresponding dose of amiodarone.

Antiarrhythmic Effects of Amiodarone and Liposomal Amiodarone

Representative electrocardiograms of the rats that received saline, free amiodarone or liposomal amiodarone are shown in Fig. 4. The intravenous administration of liposomal amiodarone (3 mg/kg), but not amiodarone (3 mg/kg), significantly reduced the duration of VT/VF compared with saline (Table 3). Furthermore, the mortality in the group that received liposomal amiodarone (3 mg/kg), but not the corresponding dose of amiodarone (3 mg/kg), was significantly lower than that in the saline group. In the group of rats that received a high dose of amiodarone (10 mg/kg), the VT/VF duration was 36±12 s, and none of the rats died (Table 3), which was similar to the low dose of liposomal amiodarone group (3 mg/kg).

Discussion

In this study, we revealed that 1) liposomal amiodarone was successfully prepared using a thin-film method, 2) the

Table 1 Characterization of liposomes by dynamic light scatter analysis

	Mean diameter (nm)	Polydispersity index	ζ Potential (mV)
PEGylated liposomes (empty liposomes)	111±14	0.124±0.027	−2.1
PEGylated liposomal amiodarone	113±8	0.128±0.040	−3.7

Results represent 4 independent experiments. The values are expressed as the mean ± SD. *PEG* polyethylene glycol

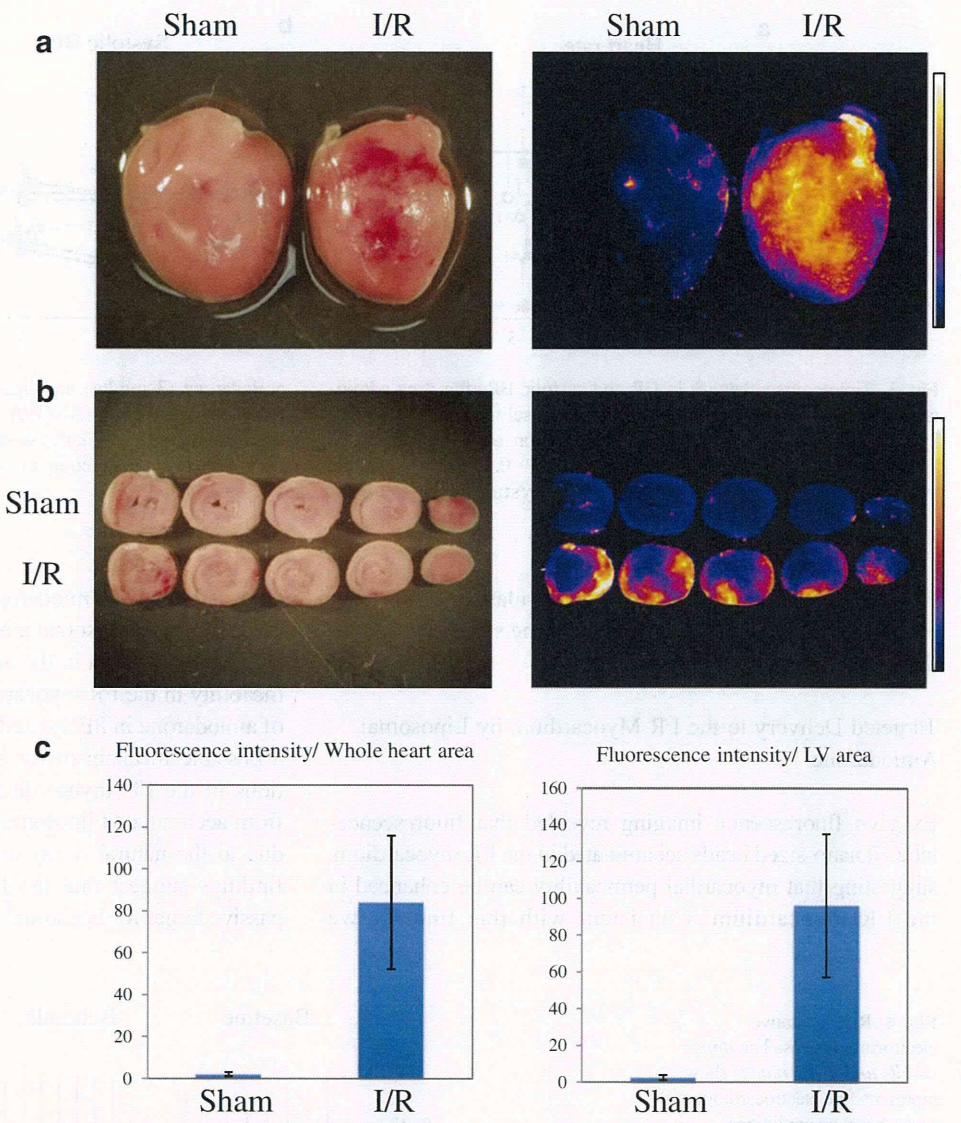

Fig. 2 Representative pictures of ischemia/reperfused myocardium with and without fluorescence-labeled nano-sized beads. Representative pictures obtained by fluorescent imaging are shown in **a** (*whole heart*) and **b** (*sliced hearts*). Quantitative analysis revealed that the average fluorescence intensity of the whole heart (**c** *left*) or the left ventricle (**c** *right*) of the I/R hearts was significantly higher than that of the sham-operated hearts

accumulation of nano-sized beads was observed in the I/R myocardium, 3) liposomal amiodarone showed a smaller reduction in the HR and systolic BP compared with free amiodarone, and 4) liposomal amiodarone, but not amiodarone, reduced the VT/VF duration and mortality during the reperfusion period compared with saline.

Table 2 Amiodarone concentration in the blood and I/R myocardium

Groups	Plasma, ng/mL	Myocardium, ng/mL
Saline	N.D.	N.D.
Free amiodarone	472±147	N.D.
Liposomal amiodarone	3872±378*	71±7*

Data are expressed as the mean ± SEM. *N.D.* not detected. $n=3$ rats in each group. * $p<0.05$ versus free amiodarone

Preparation of Liposomal Amiodarone

This study is the first to encapsulate amiodarone in PEGylated liposomes, although it has been previously encapsulated in other liposomes [22] and micelles [23]. We demonstrated that lipid bilayers composed of unsaturated lipids are more suitable for encapsulating amiodarone in PEGylated liposomes compared with those composed of saturated lipids. PEGylated liposomes have a long circulating time in the bloodstream because PEG endows a steric barrier to liposomes, allowing them to avoid interactions with opsonins and cells of the mononuclear phagocytic system [24]. Thus, they have been used to increase drug stability, safety, and bioavailability in clinical applications. In this study, we found that a higher concentration of amiodarone was retained in the blood when we administered liposomal amiodarone compared with the administration of

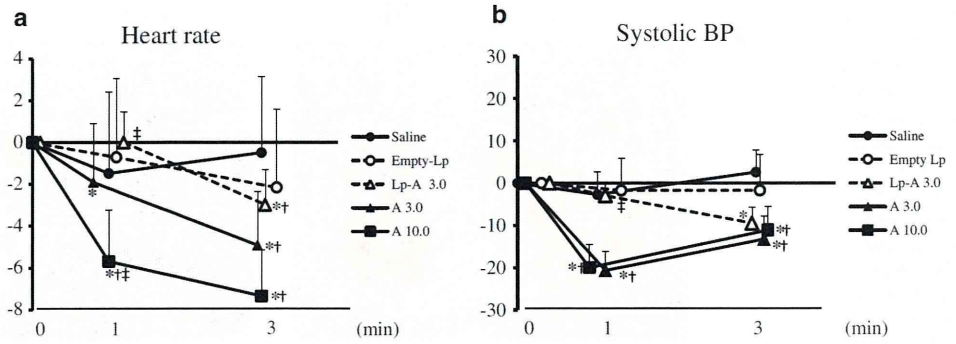

Fig. 3 Time-course changes in HR and systolic BP after drug administration. Shows the percent change from baseline for HR (**a**) and systolic BP (**b**) after intravenous administration of the tested drugs. The data are expressed as the mean ± SEM. *$P<0.05$ versus baseline, paired t-test. $P=0.0009$ (HR), 0.0002 (systolic BP) between amiodarone (3 mg/kg) and liposomal amiodarone (3 mg/kg), 1-way repeated-measurement ANOVA. †$P<0.05$ versus saline, ‡$P<0.05$ versus amiodarone (3 mg/kg), 1-way repeated-measurement ANOVA with Bonferroni's multiple comparison

free amiodarone, suggesting that encapsulation of amiodarone in PEGylated liposomes enhances the stability of amiodarone in the blood.

Targeted Delivery to the I/R Myocardium by Liposomal Amiodarone

Ex vivo fluorescence imaging revealed that fluorescence-labeled nano-sized beads accumulated in the I/R myocardium, suggesting that myocardial permeability can be enhanced in the I/R myocardium. Consistent with this finding, we observed that the amiodarone concentration in the I/R myocardium in the liposomal amiodarone group was much higher compared with that in the amiodarone group. Enhanced permeability in the I/R myocardium and the prolonged presence of amiodarone in PEGylated liposomes in the blood represent a possible mechanism for increased amiodarone concentrations in the I/R myocardium. Amiodarone will be released from accumulated liposomal amiodarone in I/R myocardium due to the natural decay and concentration gradient. These findings suggest that the I/R myocardium is a promising passive target for liposomal drug delivery.

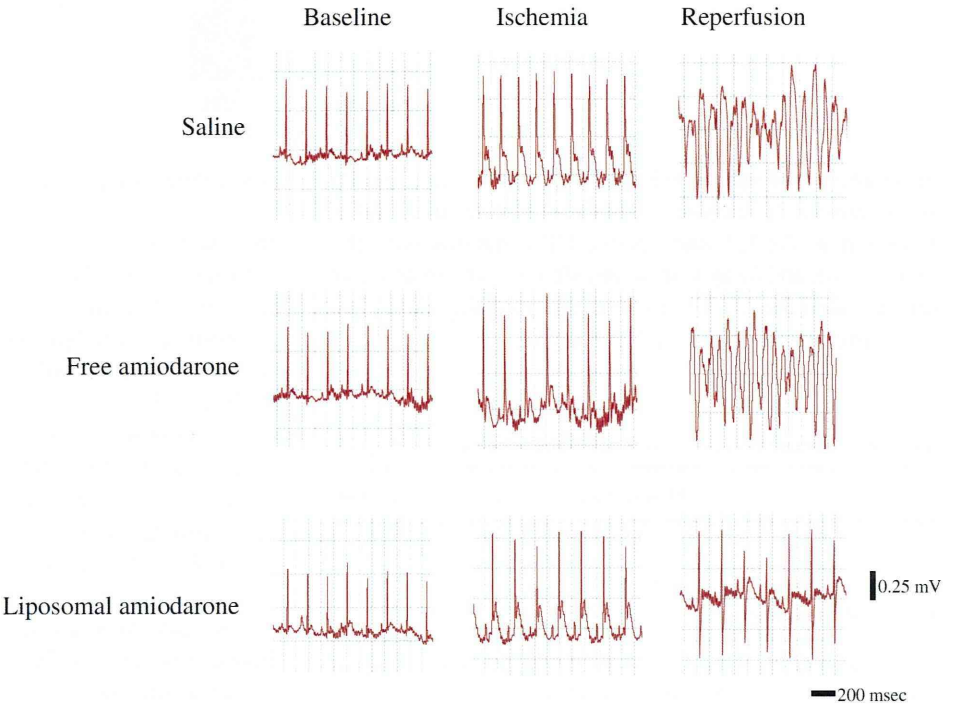

Fig. 4 Representative electrocardiograms. The *upper, middle and lower panels* show representative electrocardiograms under baseline conditions during ischemia and at the onset of reperfusion for rats that received saline, free amiodarone (3 mg/kg) and liposomal amiodarone (3 mg/kg), respectively